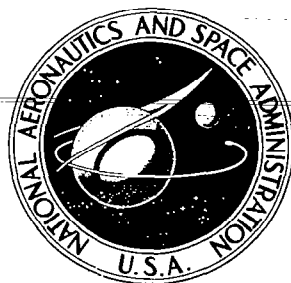


NASA CONTRACTOR  
REPORT

NASA CR-946



NASA  
CR  
935  
v.12  
c.1



LOAN COPY: RETURN TO  
AFWL (WLIL-2)  
KIRTLAND AFB, N MEX

# DYNAMIC STABILITY OF SPACE VEHICLES

Volume XII - Re-Entry Vehicle  
Landing Ability and Control

*by B. J. Kuchta*

*Prepared by*

GENERAL DYNAMICS CORPORATION

San Diego, Calif.

*for George C. Marshall Space Flight Center*



NASA CR-946

TECH LIBRARY KAFB, NM



0060029

## DYNAMIC STABILITY OF SPACE VEHICLES

### Volume XII - Re-Entry Vehicle

#### Landing Ability and Control

By B. J. Kuchta

Distribution of this report is provided in the interest of information exchange. Responsibility for the contents resides in the author or organization that prepared it.

Prepared under Contract No. NAS 8-11486 by  
GENERAL DYNAMICS CORPORATION  
San Diego, Calif.

for George C. Marshall Space Flight Center

NATIONAL AERONAUTICS AND SPACE ADMINISTRATION

---

For sale by the Clearinghouse for Federal Scientific and Technical Information  
Springfield, Virginia 22151 - CFSTI price \$3.00



## FOREWORD

This report is one of a series in the field of structural dynamics prepared under contract NAS 8-11486. The series of reports is intended to illustrate methods used to determine parameters required for the design and analysis of flight control systems of space vehicles. Below is a complete list of the reports of the series.

Volume I	Lateral Vibration Modes
Volume II	Determination of Longitudinal Vibration Modes
Volume III	Torsional Vibration Modes
Volume IV	Full Scale Testing for Flight Control Parameters
Volume V	Impedence Testing for Flight Control Parameters
Volume VI	Full Scale Dynamic Testing for Mode Determination
Volume VII	The Dynamics of Liquids in Fixed and Moving Containers
Volume VIII	Atmospheric Disturbances that Affect Flight Control Analysis
Volume IX	The Effect of Liftoff Dynamics on Launch Vehicle Stability and Control
Volume X	Exit Stability
Volume XI	Entry Disturbance and Control
Volume XII	Re-entry Vehicle Landing Ability and Control
Volume XIII	Aerodynamic Model Tests for Control Parameters Determination
Volume XIV	Testing for Booster Propellant Sloshing Parameters
Volume XV	Shell Dynamics with Special Applications to Control Problems

The work was conducted under the direction of Clyde D. Baker and George F. McDonough, Aero Astro Dynamics Laboratory, George C. Marshall Space Flight Center. The General Dynamics Convair Program was conducted under the direction of David R. Lukens.



## TABLE OF CONTENTS

<u>Section</u>	<u>Page</u>
1 INTRODUCTION . . . . .	1
2 STATE OF THE ART . . . . .	3
3 CRITERIA . . . . .	5
4 RECOMMENDED PRACTICES . . . . .	7
4.1 Low L/D Spacecraft . . . . .	7
4.1.1 Nonmaneuverable Landing Systems . . . . .	7
4.1.2 Maneuverable Landing Systems. . . . .	11
4.1.2.1 Primary Descent System . . . . .	12
4.1.2.2 Landing Rocket System . . . . .	16
4.1.2.3 Impact Attenuation System . . . . .	19
4.1.2.4 Overturn Prevention System . . . . .	21
4.1.2.5 Landing Visibility . . . . .	25
4.2 Horizontal Landing Spacecraft . . . . .	27
4.2.1 Fixed Geometry . . . . .	29
4.2.1.1 Wing Effects . . . . .	29
4.2.1.2 Fin Toe-In Effects . . . . .	30
4.2.1.3 Body Aft-End . . . . .	30
4.2.1.4 Fin Sweep . . . . .	30
4.2.1.5 Landing Criteria . . . . .	32
4.2.1.6 Landing Analysis . . . . .	34
4.2.2 Variable Geometry . . . . .	42
4.2.2.1 Switch-Blade . . . . .	43
4.2.2.2 Fold Out . . . . .	43
4.2.2.3 Single Pivot. . . . .	43
4.3 Powered Landing Spacecraft . . . . .	46
4.3.1 Propulsive Lift . . . . .	46
4.3.2 Powered Rotors . . . . .	50
5 REFERENCES . . . . .	55
 <u>Appendix</u>	
A PARACHUTE EQUATIONS OF MOTION AND STABILITY EQUATIONS . . . . .	57

## TABLE OF CONTENTS (Continued)

<u>Appendix</u>		<u>Page</u>
A.1	Assumptions . . . . .	57
A.2	Equations of Motion . . . . .	57
	A.2.1 Basic Derivation . . . . .	57
	A.2.2 Nondimensional Equations . . . . .	59
A.3	Solutions of Equations of Motion . . . . .	62
	A.3.1 Small Disturbance Analysis . . . . .	62
	A.3.2 Large Disturbance . . . . .	68

## LIST OF ILLUSTRATIONS

<u>Figure</u>		<u>Page</u>
1	Recovery Technique for Apollo . . . . .	9
2	Design Drogue Parachute System . . . . .	9
3	Drogue-Parachute Attachments Used in Deployment Tests . . . . .	9
4	Diagram for Discussion of Spacecraft Rotation Tests . . . . .	9
5	Modified Drogue Attachment Configurations . . . . .	10
6	Apollo Recovery Envelope . . . . .	11
7	Horizontal Velocity and Descent Rate Variation with Parachute Size (Nominal Sea-Level Conditions - Spacecraft Weight = 8,500 lb) . . . . .	15
8	Cloverleaf Parachute Design Performance . . . . .	16
9	Effect of Braking Rocket Thrust-to-Weight Ratio on Impact Velocity . . . . .	19
10	Landing Stability Envelope for a Rigid Ballistic Spacecraft . . . . .	23
11	Landing Stability Envelope for a Rigid Ballistic Spacecraft, Preferred Landing Orientation . . . . .	24
12	Landing Stability of Ballistic Spacecraft with Outriggers . . . . .	26
13	Ballistic Spacecraft Landing Visibility Requirements . . . . .	28
14	Effect of Wing Section . . . . .	30
15	Effect of Fin Toe-In . . . . .	31
16	Effect of Body Aft End . . . . .	31
17	Effect of Fin Sweep . . . . .	31
18	Landing Phases . . . . .	32
19	Landing Profile and Polar . . . . .	33
20	Approach Comparison for a Typical Vehicle . . . . .	36
21	Performance Variation with Approach Angle and Maximum L/D . . . . .	37
22	Landing Performance Criteria . . . . .	37
23	Approach Characteristics as Determined by Wind Loading and Touchdown Velocity . . . . .	38
24	Gust-Induced Angle Changes . . . . .	39



# LIST OF ILLUSTRATIONS (Continued)

Figure		Page
25	Demonstrated Ceiling Requirements for Unpowered Landings . . . .	41
26	Fineness Ratio 6 Elliptic Lifting Body Configuration Having Variable Position, Switch-Blade Wings . . . . .	44
27	Low-Fineness Ratio Lifting Body Configuration Having Foldout, Variable-Geometry Wings . . . . .	44
28	High-Fineness Ratio Trapezoidal Lifting Body Configuration Having Two-Position, Single Pivot Skewed Wing . . . . .	45
29	Influence of Body on $C_{L\beta}$ . . . . .	45
30	Propulsive Lift Vehicles . . . . .	47
31	PLAME Vehicle. . . . .	47
32	Typical System Requirements . . . . .	48
33	Total Control Moment as Function of Command . . . . .	49
34	PLAME Parachute System . . . . .	50
35	Rotor Landing System for One-Man Capsule, View 1 . . . . .	51
36	Rotor Landing System for One-Man Capsule, View 2 . . . . .	51
37	Rotor Landing System Operating Sequence . . . . .	53
38	Landing Maneuvers with Rotor Landing System . . . . .	53
A-1	Coordinate Systems . . . . .	58
A-2	Angle of Attack and Centroidal Lengths . . . . .	60
A-3	Statically Stable Glide. . . . .	60
A-4	Typical Force Coefficient Curves for a Parachute . . . . .	63
A-5	Nondimensional Apparent Inertia . . . . .	69
A-6	Experimental Curves for $C_{N\alpha}$ and $C_{T\alpha}$ per Radian . . . . .	69
A-7	Effects of Glide Angle on Stability. . . . .	70
A-8	Effects of Froude Number on Stability . . . . .	70
A-9	Effects of Slenderness Ratio on Stability . . . . .	71
A-10	Computer Simulation for 1°, 10° and 20° Disturbances. . . . .	72
A-11	Response to 1° and 40° Lateral Disturbance . . . . .	73

## LIST OF TABLES

<u>Table</u>		<u>Page</u>
1	Summary of the Characteristics of Maneuvering Descent Systems . . .	14
2	Propulsive Braking Systems . . . . .	17
3	Landing Attenuation Systems Comparison . . . . .	20

## 1/INTRODUCTION

A stable spacecraft configuration is required to guarantee satisfactory and safe landing on return to earth. Landing techniques range from ballistic descent trajectories with parachute recovery systems, to high lift-over-drag ratio (L/D) variable geometry vehicles or to vertical-descent, powered landing spacecraft.

All the current operational spacecraft utilize the low L/D trajectories with a parachute recovery system. This system provides a safe and reliable recovery with minimum stress and proficiency demands on the crew. However, as the present day touchdown area is over water, deployment of a large recovery force is required.

Current practice is to provide a stable configuration so that none of the crew's attention is required for stability or control on landing. This policy will not be continued on future programs because it is planned to incorporate maneuvering capability under pilot control. For these spacecraft the pilot should be furnished a stable vehicle, hands off, so that his attention will not be required to maintain stability during landing.

There will be a significant area of tradeoff when the landing configuration requirements versus re-entry requirements are considered. This monograph will consider the control and stability aspects of spacecraft just prior to and during touchdown. It will not attempt to cover vehicle configuration selection because vehicle configuration depends on total system and mission tradeoffs.

The criteria and recommended practices sections of this monograph are divided into three categories. The first discusses the landing of a low L/D spacecraft. The second discusses horizontal landing spacecraft, and the third touches on vertical descent, powered landing spacecraft.



## 2/STATE OF THE ART

The advent of spacecraft having maneuvering capability and the demonstration of the feasibility of control by the crew during re-entry flight and landing makes return to a preselected land recovery site a desirable goal. Development of a satisfactory land recovery system which is compatible with requirements for re-entry, however, is still considered a primary problem area.

The present state of the art does not allow parachute descent with touchdown on land. It is probable that the majority of future efforts will not be directed toward land touchdown of a parachute capsule but rather toward the development of a spacecraft having a horizontal landing capability. This does not, however, preclude all consideration of maneuverable spacecraft with low L/D ratios.

Development of a land recovery capability to allow normal horizontal landing on existing runways, for spacecraft having the appropriate re-entry aerodynamic characteristics, introduces further problems. In particular, many of the requirements for landing are in direct opposition to the re-entry requirements. Possible configurations for horizontal landing are being investigated. At this time one must assume the general ground rules for stability, control and handling qualities during the landing of a spacecraft will be an extension of the criteria used for high performance aircraft.

Researching the available literature on ballistic and high performance aircraft landings for definitions of the requirements and criteria for landing systems yielded considerable data for specific configurations and specific missions. However, a comprehensive criterion for spacecraft landing and recovery operation is not yet available. This report sets forth what the criteria for landing should be based upon knowledge available today. As a result many of the ground rules and requirements set forth in this monograph have not been extensively analyzed nor thoroughly tested.



### 3/CRITERIA

The current class of operational spacecraft are nonmaneuverable, low L/D types for water touchdown. These vehicles are required to be aerodynamically stable so that the pilot's attention is not required for basic capsule stability. This requirement is present at all phases of flight through re-entry and touchdown. The spacecraft re-entry and landing system must also be configured so as to limit the maximum accelerations and angular rates during this time. This will continue to be the practice for future spacecraft, both vertical descent and horizontal landing types. In addition to providing a stable capsule the spacecraft must be capable of damping out disturbances during this pre-touchdown period. A parachute landing spacecraft must also be capable of impact on the surface without overturning or excessive rebound.

When horizontal landing spacecraft are designed, the vehicle will be required to be stable, hands off, during all flight regimes. The requirement for a stable flyable vehicle will be retained for future spacecraft, but it may be relaxed to allow a stability augmentation system to be employed later. When maneuvering capability is provided consideration must be given to pilot visibility so that this capability can be fully utilized by the pilot.

The requirement for high L/D ratios during hypersonic flight, for re-entry maneuvering capability to a fixed airport, does not necessarily imply that horizontal landing is necessary or desirable. In addition, requirements for hypersonic and subsonic maneuverability are not always compatible in a fixed-geometry configuration. Variable-geometry configurations are still in the development stage. They may be realizable for spacecraft in the post-Apollo time table and therefore cannot be ignored at this time. When spacecraft having maneuvering capability during re-entry and landing are developed it is expected that they will have like handling quality requirements and be flown similarly to present day high performance aircraft - the only exception being that horizontal landing spacecraft will probably not have sufficient glide capability to use normal instrument landing procedures.

Powered assist to landing will add maneuvering and holding capability to spacecraft. Such types of spacecraft are being investigated and may in the future become practical for insertion into a re-entry capsule. Several types are discussed even though sufficient data are not available at this time to formulate meaningful criteria.

The use of autorotation rotors provides some advantages. The rotor re-entry system permits a combination of parachute-type descent with maneuvering and flaring capability. As with all other descent and landing systems, a stable system must be provided to minimize pilot attention to capsule stability during re-entry and landing.





## 4/RECOMMENDED PRACTICES

The recommended practices section of the report is broken into three major divisions. The first covers parachute or direct-descent vehicles. Next, horizontal landing spacecraft are discussed, both fixed and variable geometry. Finally the more promising types of propulsive assist to landing are discussed. A short discussion of rotor landing spacecraft is also included in this section.

The initial section is preceded by a description of the Apollo re-entry and landing system. This section is used to describe the general problem areas and constraints of a re-entry and landing system. The problems associated with re-entry are not covered in this report but are discussed in detail in Reference 1. This companion monograph discusses flying qualities and in-flight constraints in great detail.

### 4.1 LOW L/D SPACECRAFT

All of the operational spacecraft in this country are of the nonmaneuverable, low L/D type with water touchdown. However, low L/D designs are presently being considered where some landing maneuver capability has been incorporated to allow the pilot a choice of possible impact areas and to avoid local obstacles.

**4.1.1 NONMANEUVERABLE LANDING SYSTEMS.** The Mercury ( $L/D = 0$ ), Gemini ( $L/D = 0.1$ ) and Apollo ( $L/D = 0.3$ ) landing systems employ the sequence of spacecraft stabilization by drogue parachute deployment, nonmaneuverable main parachute deployment and water ballasting for overturn prevention. Since Mercury, Gemini and Apollo landing systems are similar, only the Apollo system will be discussed in this section.

In order to show the phases of the Apollo recovery that are discussed, the sequence of events for the Apollo recovery is shown in Figure 1. The first sketch on the left-hand side of the figure shows the spacecraft gliding down with the reaction controls providing stabilization. The reaction control system is the primary control used during entry. In the next sketch, the apex cover is jettisoned and the drogue parachutes are being deployed. This event occurs at an altitude of about 25,000 feet. In the third sketch the spacecraft is being decelerated and stabilized by the drogue parachutes; in the fourth sketch the drogue parachutes are jettisoned and the pilot chutes are being deployed to pull out the main parachutes. This event occurs at an altitude of about 12,000 feet, which is reached about 30 seconds after the deployment of the drogues. The final sketch shows the spacecraft descending with the main parachutes fully deployed.

The drogue parachute system is designed so that either of the two drogues can retard and stabilize the spacecraft satisfactorily; one of the drogues, therefore, is actually a backup system. It is believed, however, that both drogues should be deployed at the same time from the standpoint of reliability and also to take advantage of the added drag and stabilizing force.

The two drogues are attached to the spacecraft in an offset location, just above the main parachute deck. The center of gravity is offset from the symmetrical axis on the opposite side from the attachment point. This combination of offset center of gravity and offset attachment point results in a  $25^\circ$  tilt of the spacecraft.

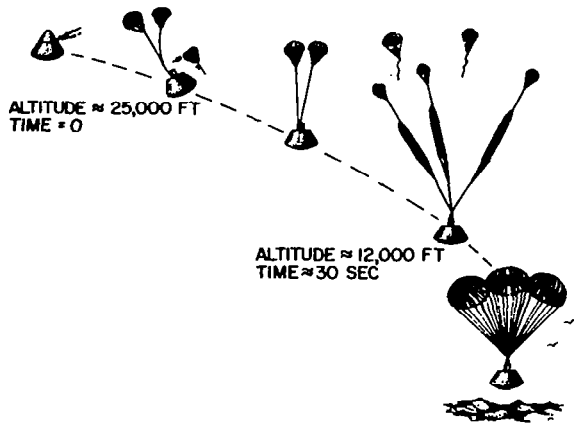
Before the deployment of the drogues, the spacecraft is stabilized by means of a reaction control system. If, however, the reaction control system should fail or run out of fuel then the basic stability of the spacecraft becomes a cause for concern. The spacecraft alone, with blunt end forward, is dynamically unstable. The instability takes the form of large oscillations and spinning.

A stability comparison has been made for two drogue-parachute attachment configurations. The left side of Figure 3 shows the one-point attachment configuration and the right side shows the four-bridle-line attachment configuration.

The stability of the spacecraft with the deployed drogues and the 1-point attachment can be erratic with the spacecraft developing large-amplitude oscillations (as high as  $\pm 30^\circ$ ) and high rotation rates about its symmetrical axis (as great as 1.1 revolutions per second). The maximum amplitudes of oscillation and the maximum rates of rotation appear to be unaffected by the number of drogues (one or two drogues). However, with one drogue the rate of build-up will be much more rapid. Since drogues are effective for only about 30 seconds prior to deployment of the main parachutes, the time for the motion to build up is important. Therefore, a two-drogue deployment is advantageous.

The fact that the motions will build up more slowly with both drogues deployed is not the result of greater stability of a clustered parachute arrangement but is the result of slower descent of the spacecraft with both drogues — that is, the airspeed will be lower so that the aerodynamic forces exciting the unstable motions will be much smaller.

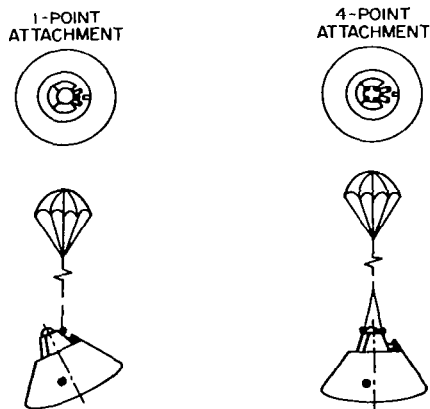
Figure 4, which is used as an aid in discussing the source of the spacecraft rotation problem, shows the one-point drogue attachment configuration. The rotation will result from the aerodynamic asymmetries caused by the tilt of the spacecraft and the offset center of gravity. As the spacecraft sideslips into or out of the plane of the figure, it will develop an aerodynamic rolling moment about the X-axis, which initiates the rotation. This aerodynamic rolling moment corresponds to the dihedral offset of an airplane.



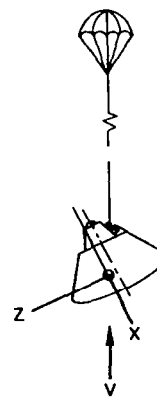
**Figure 1. Recovery Technique for Apollo**



**Figure 2. Design Drogue Parachute System**



**Figure 3. Drogue-Parachute Attachments used in Deployment Tests**



**Figure 4. Diagram for Discussion of Spacecraft Rotation Tests**

A spacecraft with its center of gravity on the symmetrical axis will not have this tendency to rotate. However, the offset of center of gravity is a requirement of the hypersonic region of entry flight.

As the number of drogue attach points increases, the stability of the spacecraft increases. Figure 5 shows some of the other attachment systems.

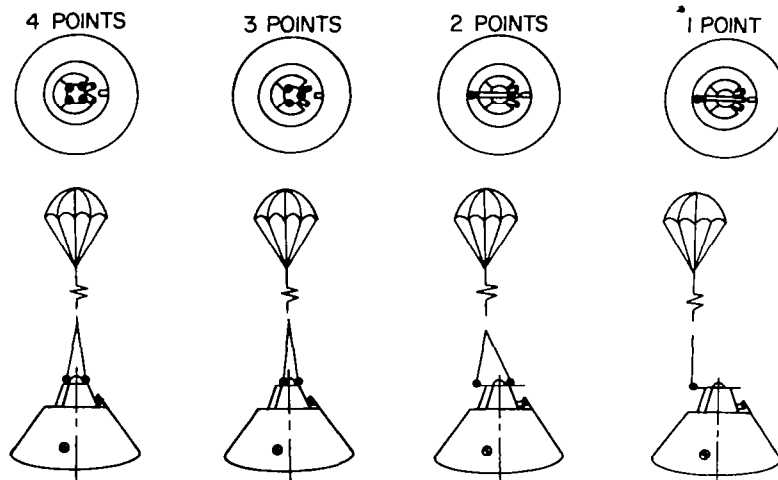


Figure 5. Modified Drogue Attachment Configurations

The 3- and 4-point attachment configurations will be considerably better than the 1- or 2-point attachment configurations. With the 3- and 4-point bridle attachment configurations spacecraft oscillations can be reduced to  $\pm 5^\circ$  maximum amplitude and the rotation rate to 0.10 revolution per second.

The recovery envelope within which the parachute system for the Apollo is required to function is defined generally in Figure 6 in terms of altitude and Mach number. It may be seen that the drogues are required to deploy over very broad ranges of altitude and dynamic pressure. The main parachute deployment envelope is understandably not as broad.

For deployment of the main chute the drogues are released and the three piloted chutes are simultaneously deployed. The pilots subsequently deploy the three main chutes in the reefed condition. Six seconds after line stretch, the main parachutes are disreefed. Eight to ten minutes later, impact occurs at a vertical velocity of about 24 fps. Failure of one main parachute can be tolerated without jeopardizing the crew.

Several general conclusions can be made about the stability of large parachutes:

- a. A parachute system which is glide-stable will damp out small longitudinal glide-point disturbances and be neutrally stable for small lateral fluctuations.

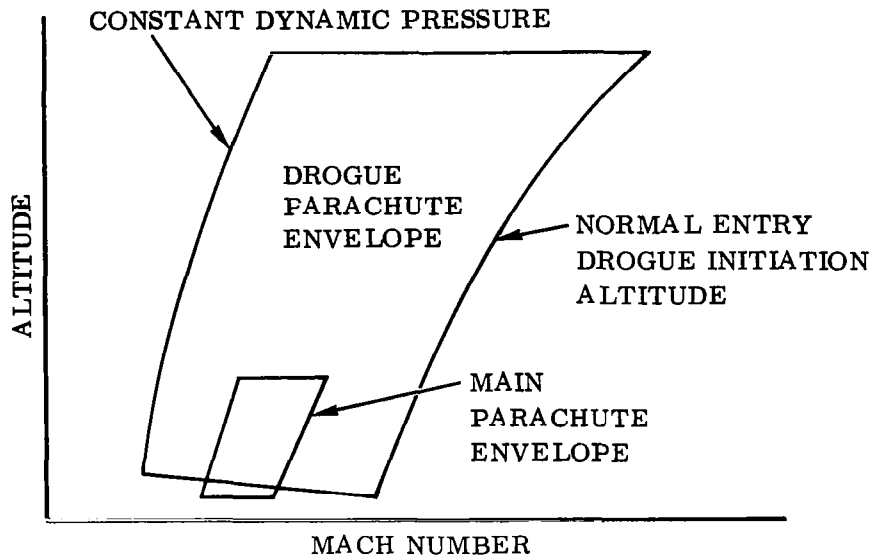


Figure 6. Apollo Recovery Envelope

- b. A system which is glide-unstable will diverge to a large angle pitching oscillation if disturbed longitudinally and to a large angle vertical coning motion if disturbed laterally.
- c. A stable parachute with finite glide point angle of attack will jump into a pitching oscillation if hit with a large longitudinal disturbance and will jump into vertical coning if struck by a large lateral displacement.

The three-dimensional motion of a freely descending parachute can be studied with a five-degree-of-freedom analysis (the roll motion is neglected). Appendix A presents the equations of motion in non-dimensionalized form for a parachute system and discusses the resulting parameters.

**4.1.2 MANEUVERABLE LANDING SYSTEMS.** The operational spacecraft of this country — Mercury, Gemini and Apollo — are all designed for one flight and to land on water with no maneuverability provided to spot-land the craft. Recent studies have been conducted to determine the stability and control requirements for a reusable ballistic spacecraft which can land at a preselected land recovery site. A preselected land recovery site implies that the guidance error accumulated from de-orbit can be closed out by low altitude maneuvering capability designed into the spacecraft. This low altitude maneuvering capability must be provided either by having a low speed  $L/D$  greater than some threshold or by providing propulsive thrust.

A footprint display of the landing zone attainable relative to the desired land site must be provided to the pilot. Present navigational and energy management systems have sufficient accuracy to compute this footprint. The best approach for determining these requirements at landing is to consider the subsystems which make up the landing system. The subsystems to consider and their function are:

- a. Primary Descent System. Stabilization of the spacecraft and reduction of the sink rate and horizontal velocity to values consistent with the remaining subsystem capability and overall system requirements.
- b. Braking Rocket System. Reduction of the sink rate from that provided by the parachute to a value compatible with the impact attenuation system and allowable impact load levels.
- c. Impact Attenuation Systems. Absorption of the energy remaining at impact without exceeding the allowable deceleration levels.
- d. Overturn Prevention System. Prevention of tumbling on impact and avoidance of the resulting damage to the spacecraft and possible injury to the crew.
- e. Landing Visibility. Although not a system, per se, consideration must be given to visibility to allow pilot to maneuver to avoid obstacles in the landing area.

The requirement for reusability imposes a 4g impact load limit for structural integrity of the spacecraft in normal landing situations. The emergency impact load limit is 20g based on human tolerance defined in Reference 2.

The primary land landing area is assumed to be circular with level terrain, at an elevation of under 2,500 feet with less than 5 percent of the area obstructed. The terrain slope for a normal landing is assumed to be no greater than 5 degrees with surface winds no greater than 20 knots.

Another requirement is for landing capability on both land and water. Normal water landings are assumed to be in relatively mild sea conditions (Sea State 3) with wave slopes no greater than 5 degrees and swells of 6 feet or less.

Emergency landing conditions may result in landing on rough water, on rough terrain, or in high winds. Elevations up to 5000 feet, winds up to 30 knots, and 10-degree wave slopes and 9-foot swells (Sea State 4) should be considered for emergency conditions.

4.1.2.1 Primary Descent System. The primary descent system is required to stabilize the spacecraft at a terminal descent rate which, in combination with the other landing subsystems, produce impact loads of 4g or less. In addition, this subsystem must provide the maneuvering capability to allow the pilot a choice of possible impact areas.

Several concepts have been put forth for a maneuvering descent system. Some are:

- a. Steerable Cloverleaf Parachute,  $L/D = 0.7$  to  $1.8$ .
- b. Parasail Parachute,  $L/D = 1.1$ .
- c. Glidesail Parachute,  $L/D = 0.5$  to  $0.6$ .
- d. Ringsail Parachute,  $L/D = 0$ .
- e. Stabilization Drogue Parachute Only,  $L/D = 0$ .
- f. Paraglider,  $L/D = 2.5$  to  $3$ .
- g. Rotors,  $L/D = 4$ .
- h. Paravulcoon.

Table 1 presents an overall summary of the characteristics of each system.




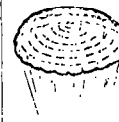

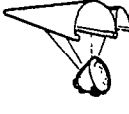

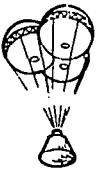
Some type of gliding parachute is the most feasible system to consider. The more exotic descent systems, such as the paraglider or rotors, provide more aerodynamic performance capability than is required for the ballistic spacecraft, at the expense of additional weight, unusable volume and complexity. Extensive development work is needed to assure reliable deployment under operational conditions of such systems as rotor, paraglider and paravulcoon.

The primary descent systems that will be discussed are the three gliding parachute types.

Parachute size is determined by the spacecraft weight, sink-rate and horizontal velocity envelope of the parachute-spacecraft system and expected wind velocities. Consideration should be given to wind velocities of zero to 30 knots. Figure 7 illustrates these effects for nominal sea level condition and for a spacecraft of 8500 lb. Data from Reference 3 for the cloverleaf parachute, Reference 4 for the ringsail, Reference 5 and 6 for the glidesail and unpublished data from NASA (MSC) for the parasail were used. Figure 7 indicates that the cloverleaf parachute has the slowest horizontal velocity envelope due to a large usable range of  $L/D$ . It can also maintain a constant sink rate through a large  $L/D$  range as shown in Figure 8. The constant sink rate is advantageous because it allows a much simpler design and lower tolerances for the rocket braking system than are required when varying descent velocities are used. The performance data in Figure 8 are shown as a function of  $W/S$ , which is the system weight divided by the projected area of the lifting surface.  $W/S$  is in effect an average pressure acting on the lifting surface.

The parasail parachute has a  $L/D$  of approximately 1.1. However, unlike the cloverleaf, the  $L/D$  of the parasail cannot be modulated through an appreciable range

Table 1. Summary of the Characteristics of Maneuvering Descent Systems

SYSTEM	CLOVERLEAF STEERABLE PARACHUTE L/D = 0.8 TO 1.8	PARASAIL L/D = 1.1	GLIDESAIL L/D = 0.6 CLUSTER OF 3	RINGSAIL L/D = 0 CLUSTER OF 3	SMALL STABILIZING PARACHUTE (NO MAIN CHUTE)	PARAGLIDER	ROTORS	PARAVULCOON
CHARACTERISTICS								
Deployment	FAIR High opening loads. May require 2- stage reefing	FAIR Large chute	FAIR Multiple chute de- ployment	FAIR Multiple chute de- ployment	GOOD Simple parachute deployment	POOR Severe deploy- ment problems	POOR Bulky and complex	POOR Bulky and complex
Complexity and Reliability	POOR Complex control system required	FAIR Complex control system	FAIR Complex control system	GOOD Simple	GOOD Simple reliable system	POOR Complex deploy- ment & control problems	POOR Anti-torque de- vice required	POOR Potential fire or explosion hazard
Parachute Weight Per Unit R/S	GOOD High L/D allows small chute diameter	POOR Large diameter. Low porosity parachute	FAIR Lighter than ring- sail	FAIR Low $C_D$ and zero lift result in large diameter chutes	GOOD Lightest possible descent system	POOR Heavier than gliding para- chutes	POOR Extremely heavy system	POOR Heavier than gliding para- chutes
Wind Cancellation	GOOD Good L/D range	FAIR Good L/D but not variable	FAIR Low L/D	POOR None	POOR No wind cancella- tion	GOOD High L/D = 2.5. Partial flare capability	GOOD Excellent L/D = 4	POOR No steering capability
Maneuver Capability	GOOD High L/D ratio, fast response	GOOD Good L/D, fair response	FAIR Slow response, Low L/D	POOR None	POOR No maneuver capability	GOOD Good turn rate and fair stability	GOOD Excellent man- euver capability and rate of des- cent control	FAIR Low rate of des- cent but no man- euver capability
Back-up	POOR Separate back-up system required	POOR Separate back-up system required	GOOD Can be clustered for redundancy	GOOD Can be clustered for redundancy	GOOD Redundant drogue, can be clustered	POOR Requires auxil- iary system	POOR Requires auxil- iary system	GOOD Cluster system provides redun- dancy
Development	POOR Preliminary stages. Small chutes	FAIR Development in advanced stages	FAIR Well developed	GOOD Well developed. Large chutes	GOOD Well tested system	POOR Extensive devel- opment effort re- quired for deploy- ment and stability	POOR Extensive devel- opment required for stowage & de- ployment	FAIR Partial develop- ment on smaller scale
General Comment	Selected system - adequate time for development		Could be best sys- tem with a good overturn stability device.		Must be used with a large rocket braking system & with an overturn prevention device.	Rejected because of severe deploy- ment problems, potential for fu- ture applications.	Requires much development ef- fort.	No specific ad- vantages not provided by an- other system.



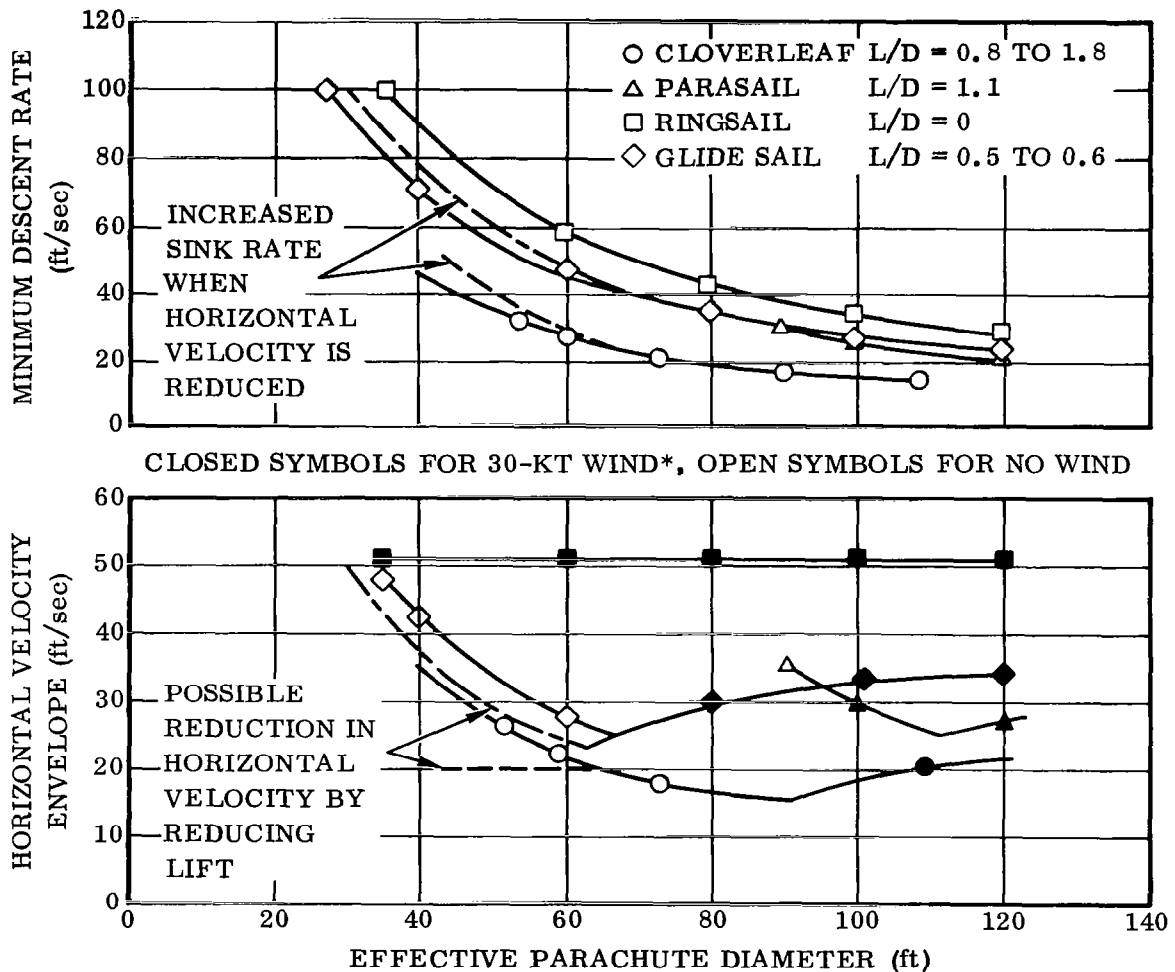


Figure 7. Horizontal Velocity and Descent Rate Variation with Parachute Size  
(Nominal Sea-Level Conditions — Spacecraft Weight = 8,500 lb)\*

\*Represents landing in the presence of a 30-knot horizontal steady-state wind.

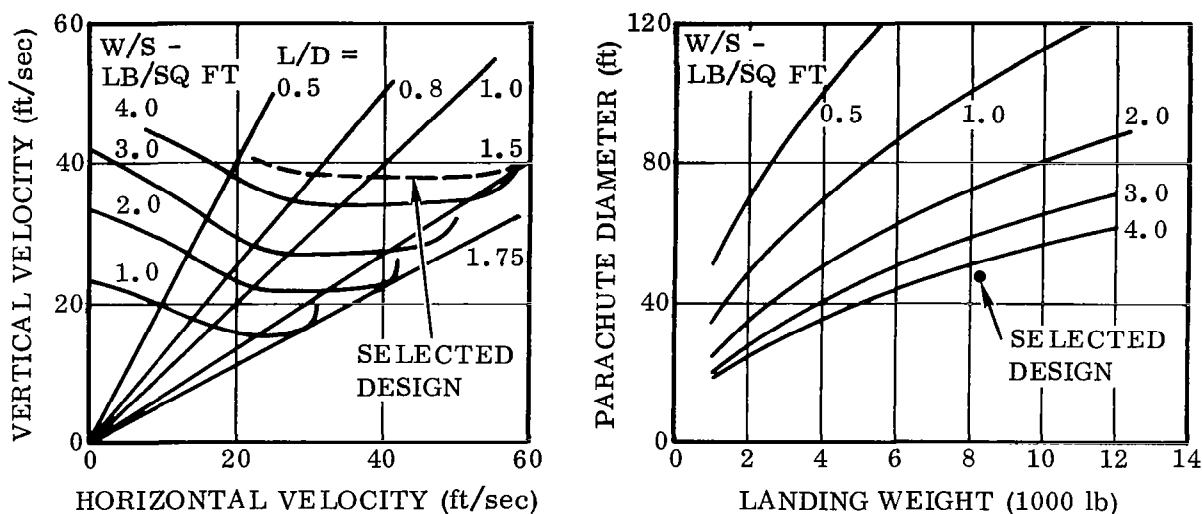


Figure 8. Cloverleaf Parachute Design Performance

while maintaining a relatively constant descent rate. As a result, very large parasail sizes are necessary to obtain low horizontal velocities in zero-wind conditions.

The glidesail has a much lower  $L/D$  than either the cloverleaf or the parasail, and has relatively poor response characteristics. However, the glidesail has several important advantages relative to the cloverleaf and parasail. These include:

- a. Clustering capability.
- b. Small size required to obtain minimum horizontal velocity.

The parasail has less maneuverability and glide capability than the lighter, less complex cloverleaf parachute. The glidesail has sufficient maneuver capability to avoid local terrain hazards.

**4.1.2.2 Landing Rocket System.** Liquid and solid propellant systems with various mounting, deployment and actuation techniques can be considered for land rocket systems. Table 2 summarizes a variety of concepts.

Liquid propellant systems are relatively easy to throttle, can be gimbaled, and have shutdown capability. As a result, almost zero touchdown velocity can be obtained. However, the liquid system is complex, creates storage problems, is heavy and is a potential crew hazard in case of an inadvertent high impact load.

Table 2. Propulsive Braking Systems

SYSTEM	DEPLOYMENT	STOWAGE	WEIGHT	THRUST TERMINATION	STABILITY	CHUTE INTERFERENCE	GROUND EFFECTS	GENERAL COMMENT
Riser-Mounted Solid Motor	FAIR	FAIR	GOOD	FAIR	GOOD	FAIR	GOOD	Selected system
	Complicates back-up chute rising	Small volume available in cone apex	Small structural weight. No ballast	(Jettison)	Flexible tractor through c.g.	Possible suspension line heating	None	
Skirt-Mounted Solid Motor	GOOD	GOOD	FAIR	POOR	POOR	GOOD	POOR	Fixed heat shield creates deploy- ment problems
	Not required with extend- ible heat shield	Fixed in- stallation between heat shield and pres- sure shell	Added structural weight re- quires ballast	Added complication	Thrust not through c.g.	None	Direct ground impingement	
Centerline, Base-Mounted Solid Motor	GOOD	FAIR	FAIR	POOR	FAIR	GOOD	POOR	Direct impingement
	Blow out hole in heat shield	Potential hazard to crew	Structural weight penalty. Increased ballast	Added complexity	Rigid pusher sensitive to c.g. tolerance	None	Direct impingement	
Centerline, Base-Mounted Liquid-Propel- lant System	GOOD	POOR	POOR	GOOD	GOOD	GOOD	POOR	Would eliminate concern for horizontal velocity
	Jettison heat shield	Large volume. Penetrates crew module	Large inert weights	Throttleable	Gimballed nozzle	None	Direct impingement	

Solid-propellant motors provide a high thrust, low volume, high reliability system. However, the primary disadvantage is that tolerance error corrections are more difficult due to the fixed thrust and total impulse characteristics.

Three concepts can be considered for rocket motor installation:

- a. Base-mounted motor installed on the longitudinal centerline.
- b. Multiple motors installed around the base perimeter.
- c. Parachute riser-mounted motors.

The base-mounted centerline motor has the advantage of aligning the thrust vector through the center of gravity. However, the motor exhaust would create ground effect problems.

Installation of motors along the base perimeter results in ground effect problems, and stability problems arise from the inability to align the thrust vector through the center of gravity without incurring prohibitively high nozzle-cant angles.

Mounting on the parachute risers provides the advantage of no ground effects and an inherently stable system. These advantages result from the ability to fire through the center of gravity and the flexible motor suspension that corrects automatically for thrust vector — c.g. misalignment. The major disadvantage of this mounting is that the exhaust impinges on both the spacecraft and the risers.

The landing rockets should be sized for a potential range of parachute terminal velocity of 20 to 100 ft/sec. The burn-time of the motor main stage should be long enough to provide a maximum  $\Delta V$  equal to the minimum parachute sink rate. Shorter burn times result in higher impact velocities. A longer burn-time could result in reversal of spacecraft velocity and termination of main motor operation at a greater distance off the ground than at ignition. Figure 9 shows thrust-to-weight ratio versus impact velocity for several parachute velocities. These curves were generated from the following expression:

$$\text{IMPACT VELOCITY} = \sqrt{V_o^2 + 2 hg (1-T/W)}$$

where:

$h$  = Motor ignition altitude

$V_o$  = Parachute velocity

$T/W$  = Thrust-to-weight ratio

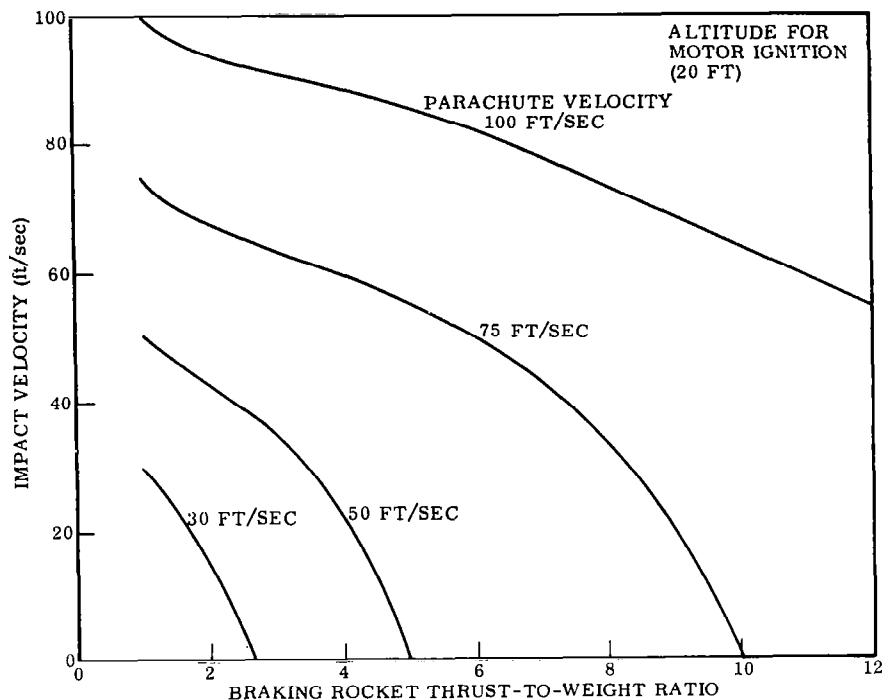


Figure 9. Effect of Braking Rocket Thrust-to-Weight Ratio on Impact Velocity

It should be noted that Figure 9 was generated for a fixed ignition altitude. A radar altimeter could provide the altitude intelligence data for ignition. The thrust vector for the braking rocket is assumed to pass through the vehicle center of gravity; therefore, no appreciable disturbing moments will be produced by the braking rocket thrust, and an attitude control system is not necessary.





**4.1.2.3 Impact Attenuation System.** Many impact attenuation devices have been proposed. Four possible systems are:

- a. Fixed heat shield.
- b. Extended heat shield.
- c. Extended vertical landing gear.
- d. Extended Gemini type landing gear.

Table 3 summarizes these four systems.

For the fixed heat shield system a titanium honeycomb covers approximately one-half of the heat shield area and provides the mean of attenuating the landing impact loads. The honeycomb is bonded to the inner pressure walls, which are supported on a number of beams that are positioned in a waffle pattern to offer the maximum support.

Table 3. Landing Attenuation Systems Comparison

SYSTEM CHARACTERISTICS	FIXED HEAT SHIELD	EXTENDIBLE HEAT SHIELD	EXTENDIBLE LANDING GEAR VERTICAL SYSTEM	EXTENDIBLE LANDING GEAR GEMINI TYPE
				
Weight	FAIR	GOOD	POOR	POOR
	•Medium weight system	•Lightest system	•Heavy weight system	•Heaviest weight system
Complexity	GOOD	FAIR	FAIR	FAIR
	•Simplest of all systems •Most reliable	•System requires operation of three sequential actuation subsystems	•System requires operation of three sequential actuation subsystems	•System requires operation of four sequential actuation subsystems
Stowage and Deployment	GOOD	FAIR	FAIR	FAIR
	•No deployment required •Stowage no problem unless honeycomb depth for limiting g's becomes excessive	•Stowage of horizontal energy absorbers may be problem •Multiple systems pose sequence deployment problem	•Stowage may pose problem •Multiple systems may pose deployment problem	•Stowage may pose problem •Multiple systems may pose deployment problem
Flexibility	GOOD	FAIR	FAIR	POOR
	•Systems orientation not required •Can assist in water landings	•System orientation not required •Can assist in water landings for initial impact •May have problem with high horizontal velocity	•System orientation not required •Limited effectiveness in water landing	•System requires definite orientation •Horizontal wind velocity may be problem •May not be able to use minimum weight parachute system
Remarks	<u>Preferred System</u> •Weight is not excessive •Reliability is maximum •Completely passive system •Overturn prevention requirements depend on parachute used	•Lightest system •Requires maximum number of subsystems to function properly •Overturn prevention requirements depend on parachute used	•Among lightest systems •Requires several activation systems to function properly •No overturn prevention devices needed	•Requires several activation systems to function properly •Directional parachute required, must have forward velocity at all times •No overturn prevention device needed

The extendible heat shield system is an active subsystem that is required to:

- a. Extend the heat shield.
- b. React to vertical loads.
- c. React to horizontal loads.

The shield is supported by vertical hydraulic actuators equally spaced around the circumferential periphery. In addition, there are horizontal actuators for horizontal loads.

The extendible landing gear-vertical system consists of four 3-strut type gears with a pad attached to each. The three legs of each gear system contain crushable honeycomb, providing capability of resisting compression loads in each of the legs. This concept requires the use of three action subsystems to:

- a. Open the door of the gear housing.
- b. Extend the landing gear by pyrotechnic devices.
- c. Lock the gear in position.

This system appears to be insensitive to variation in terrain.

The extendible landing gear proposed for Gemini consists of two main gears with rectangular skids and a nose gear with a dishpan skid. The coefficient of friction of the main gear was selected to exceed that of the nose gear to provide directional stability during slide out. This system requires four active subsystems to:

- a. Open the gear housing door.
- b. Extend the gear.
- c. React the vertical reactions.
- d. React the drag reactions.

This system does not require a supplemental overturn prevention system when used with steerable parachutes that have directional landing capability.

**4.1.2.4 Overturn Prevention System.** A problem associated with the ballistic spacecraft landing system is the possibility of overturn following impact. Spacecraft overturn must be held to a minimum following normal landings to prevent injury to the crew and to minimize spacecraft damage.

The primary factors affecting overturn stability following ground impact are:

- a. Touchdown velocities.
- b. Touchdown attitude.
- c. Dynamic coefficient of friction between the landing system and the landing surface.
- d. Ground slope.
- e. Spacecraft center of gravity.
- f. Spacecraft mass and mass moment of inertia.
- g. Landing system geometric characteristics.

A stability analysis based on solution of the equations of motion which include all of the above factors can be performed. However, useful trends can be obtained by treating the spacecraft as a rigid body and analyzing the landing impact by impulse-momentum analysis, then making an overall energy check to determine overturning stability. After touchdown, it is assumed that the vehicle remains in contact with the landing surface, i. e., no rebound.

The direction of the horizontal touchdown velocity in general cannot be controlled. Analytical results consistent with this limitation are presented as stability envelopes of vertical touchdown velocity versus horizontal touchdown velocity for two dynamic coefficients of friction. Landing attitude to consider are from plus six to minus nine degrees without ground slope and with no rotational velocity at impact. These stability envelopes and a figure defining a planar model are shown in Figure 10. This envelope is also approximately correct for landing at attitude between zero and minus three degrees on ground slopes of plus or minus five degrees. When the direction of the horizontal velocity at touchdown is not controlled, the greatest stability margin is obtained for a descent attitude such that a line through the heat shield center of curvature and the spacecraft c.g. is parallel to the local vertical.

When certain parachute systems are used, both the direction and magnitude of the horizontal touchdown velocity can be controlled within limits. Figure 11 presents a composite stability envelope for the model landing with forward c.g., at attitude between -10 and -13 degrees, without ground slope, for dynamic coefficients of friction from 0.4 to 0.8. Figure 11 presents stability envelopes of vertical touchdown velocity versus landing attitude for a model rocking and sliding with c.g. forward, for dynamic coefficients of friction equal to 0.4 and 0.8 and zero ground slope. These envelopes are independent of horizontal touchdown velocity. For a combination of vertical touchdown velocity and landing attitudes lying within the cross-hatched area, any value of positive horizontal touchdown velocity will result in a stable landing.

The stability boundaries presented represent type characteristics for a typical system. Because they are difficult to predict, geometry changes due to impact loads and any residual landing rocket forces were not considered in the analysis performed to obtain the data presented.



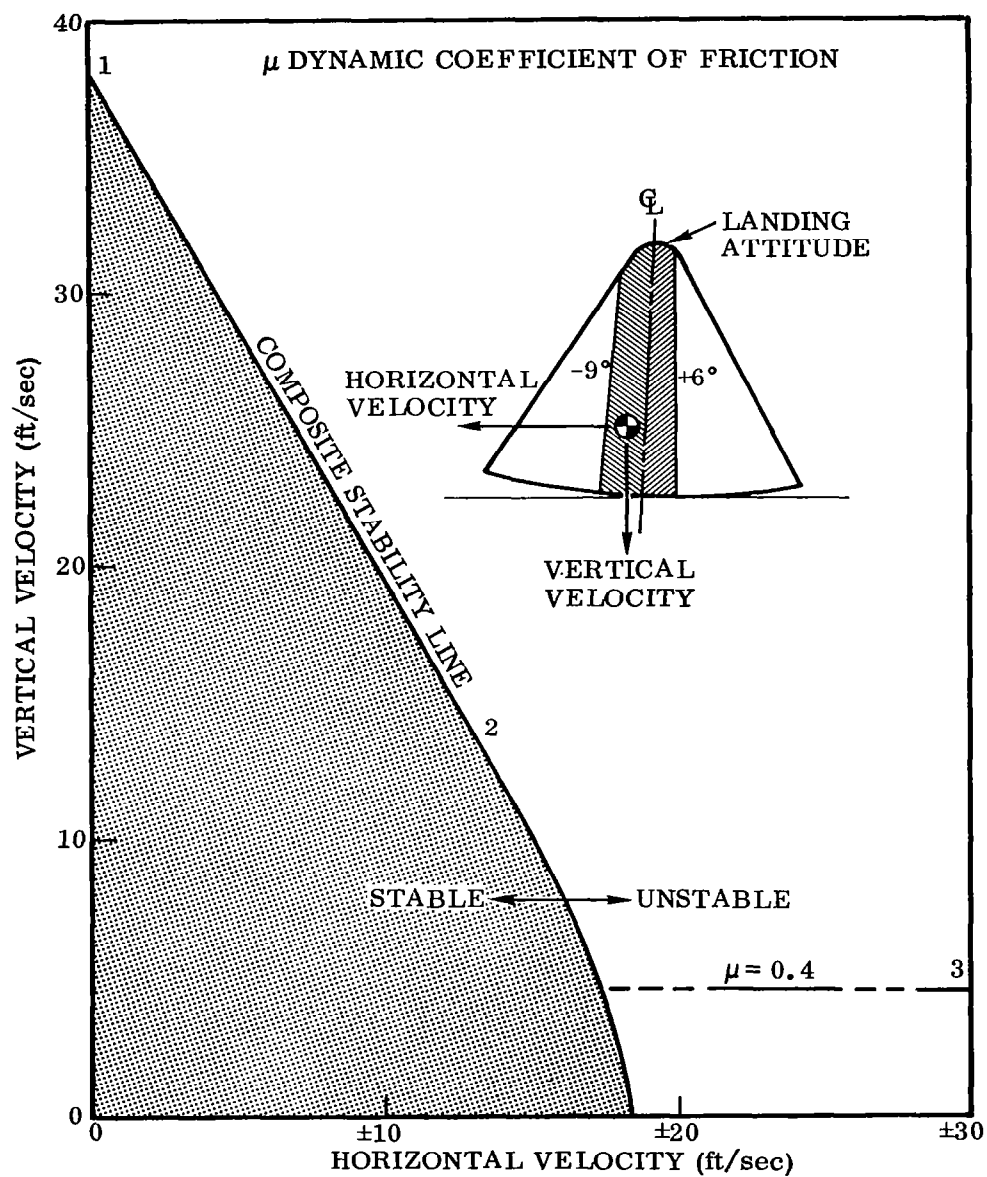


Figure 10. Landing Stability Envelope for a Rigid Ballistic Spacecraft

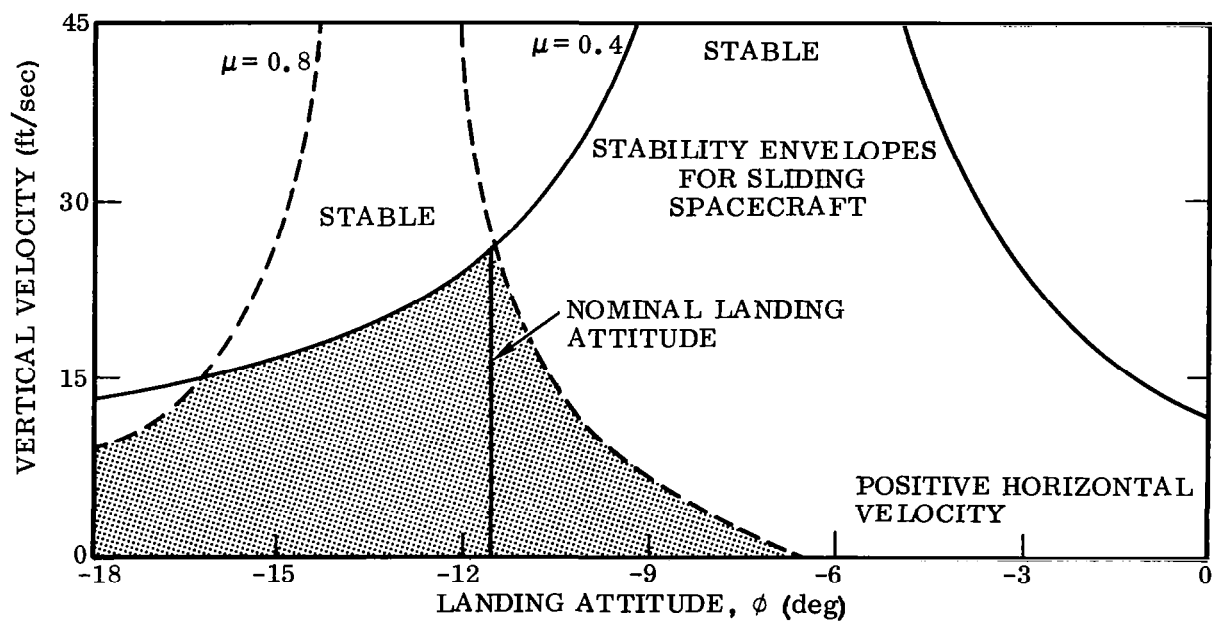
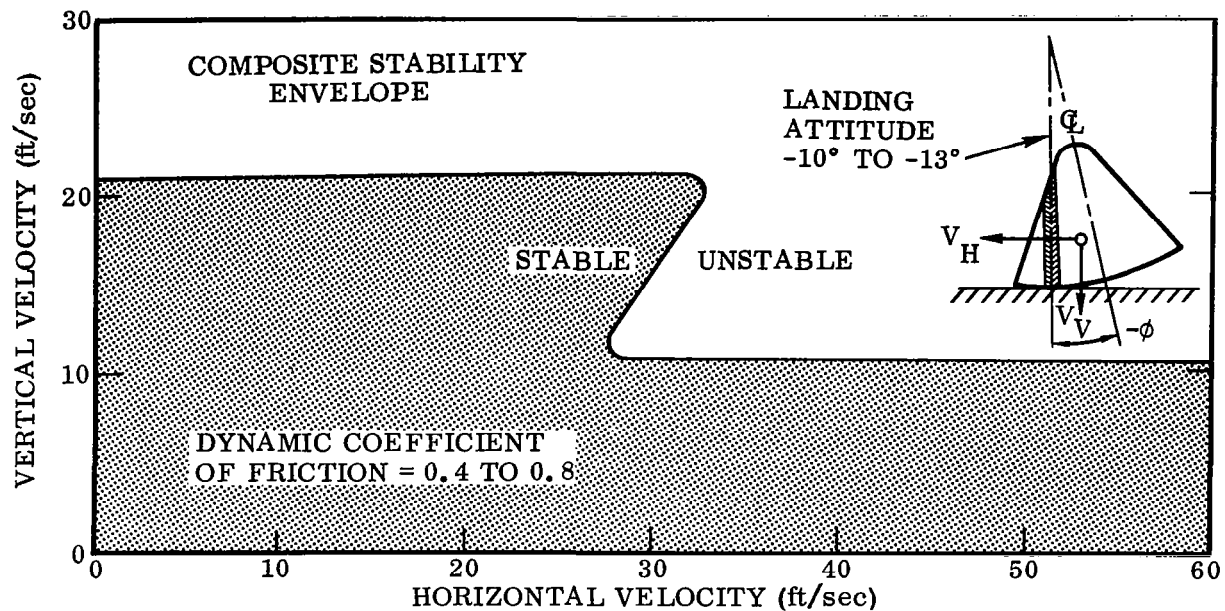


Figure 11. Landing Stability Envelope for a Rigid Ballistic Spacecraft, Preferred Landing Orientation

A positive means of increasing the overturn stability margin is to provide an overturn prevention system. Several concepts for overturn prevention are:

- a. Extendible outrigger.
- b. Extendible rollers.
- c. Extendible flap.
- d. Harpoon ground anchor.
- e. Horizontal thrusting solid rockets.

The simplest system is the extendible outriggers. Figure 12 presents curves which indicate how the maximum allowable horizontal touchdown velocity varies with outrigger length. The curve designated "Zero Percent Horizontal Velocity Dissipated" can be generated by determining the energy, attributable to the minimum horizontal touchdown velocity, which will overturn the spacecraft. The curve designated "37 Percent Horizontal Velocity Dissipated" was similarly developed except that 37 percent of the horizontal velocity is assumed to be dissipated upon impact.

For the horizontal rockets mounted on the cone apex the motors will fire until the spacecraft has stopped sliding. The motors must be controlled to balance out the moment produced about the spacecraft c.g. by the sliding friction force. Because of the uncertainty in the sliding friction coefficient an active control system must be used.

The extendible roller overturn prevention system is a simple system, but sizing the roller so that allowable landing surface bearing pressure is not exceeded may be a problem.

The harpoon ground anchor does not necessarily require a specific orientation although the rotational rates imparted to the spacecraft might be severe without proper orientation. The primary disadvantage of this system is the requirement for accurate attitude sensing and the probability of increasing the vertical impact velocity.

4.1.2.5 Landing Visibility. The landing vision requirements of the ballistic (low L/D) spacecraft are less severe than those for the horizontal landing spacecraft because the piloting task is less demanding. Lower velocities are involved and a precise landing maneuver is not required. However, it is necessary to provide a sufficient field of view to allow the pilot to maneuver the spacecraft to avoid any obstructions in the landing area. An angular field of vision of at least 120 degrees is required to cover the entire landing area for a typical system such as the cloverleaf system.

If the landing gear system is of the extended Gemini type then landing area vision can be provided through the window ports. However, for spacecraft which impact

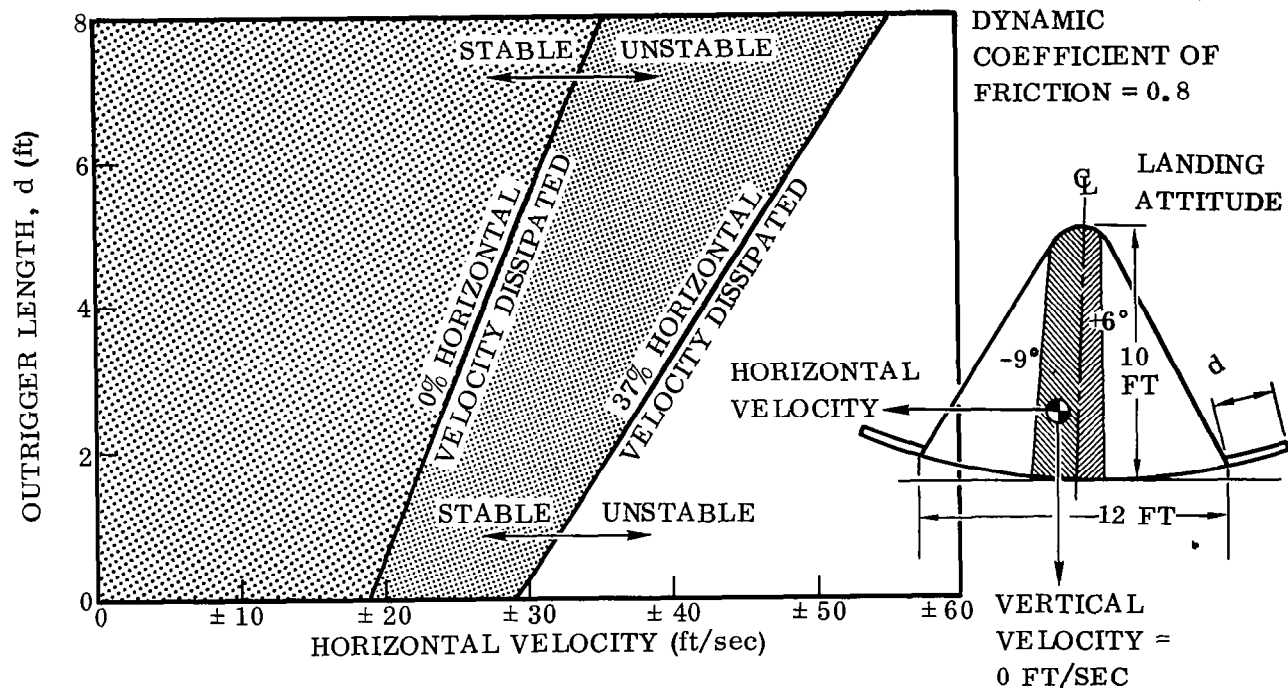


Figure 12. Landing Stability of Ballistic Spacecraft with Outriggers

in an upright attitude (heat shield down) it is almost impossible to provide direct vision with window ports. Therefore, provision of optical or electronic visual aids is required.

Two concepts which can provide vision for vertical landings are:

- a. A retractable, one-power optical periscope which projects an image in a spherical mirror in front of the pilot. The mirror is a storable device.
- b. A retractable television transmitter and an instrument panel-mounted TV display.

During the terminal descent, the pilot must be able to monitor the attitude and rate of descent during landings. For normal landings, it is desirable to limit the horizontal velocity to 30 ft per sec or less at touchdown. This requirement limits the parachute to an L/D of 0.76 under no-wind conditions and give a horizontal range as shown in Figure 13. Under this condition, a visual angle of 70 degrees encompasses the entire landing footprint area. However, a 90-degree angular field of vision can provide the pilot an extra advantage in choosing a safe landing area.

#### 4.2 HORIZONTAL LANDING SPACECRAFT

There is a tendency to read into arguments for increased hypersonic lift-to-drag ratio a justification for conventional horizontal landing. The interest that past conceptual studies of moderate to high L/D vehicles have shown in conventional landing is not surprising, and represents not so much a failure to recognize that spacecraft are not aircraft as an acknowledgement of the experience that exists in the landing of high-speed aircraft and confidence in the ability to apply it to entry vehicles.

The extent to which this is sound philosophy and appropriate to the moderate L/D class is being explored in NASA's current program involving B-52 drops of two manned vehicles, the M2-F2 and the HL-10, and in the Air Force's current SV-5. The technology evolving from these programs, coupled with related aircraft experience, may be expected to generate strong support for the conventional landing mode. However, it is premature to conclude that this is the preferred mode, particularly in the long-range view.

For vehicles conceived to fly in the conventional sense during the entire entry and to land in the manner of aircraft, aerodynamic features must be tailored for both hypersonic and low-speed flight. This involves conflicting desires and results in some compromise in either performance or weight. Vehicles having the descent and landing mode essentially decoupled from further dependence on the vehicle's continued aerodynamic flight circumvent in large part the hypersonic-subsonic compatibility problem. For the horizontal landing spacecraft a semi-decoupled approach is the deployment of stowed wings at subsonic speeds; this is not a decoupled mode in the usual sense, since the subsonic aerodynamic characteristics remain strongly governed by

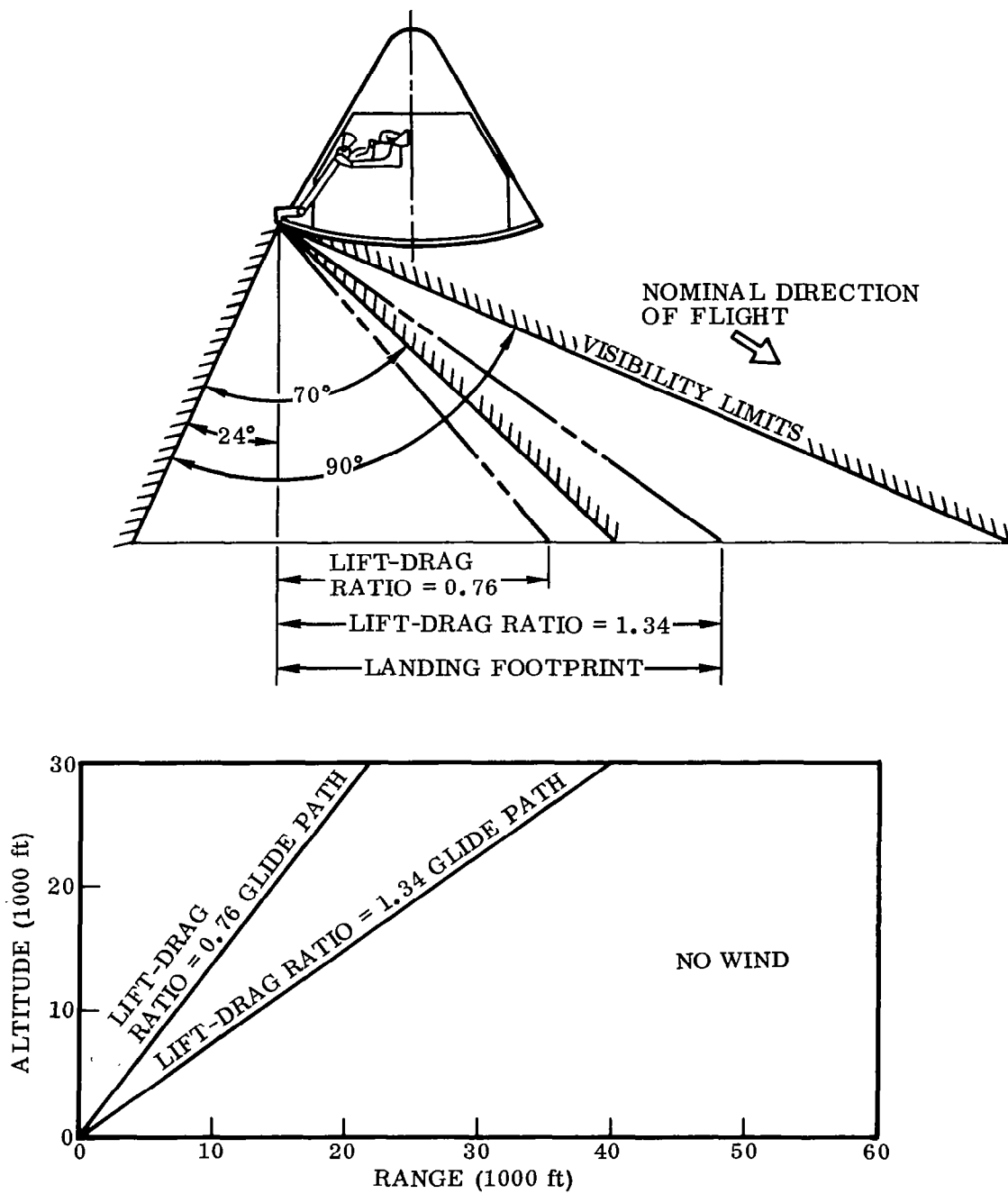


Figure 13. Ballistic Spacecraft Landing Visibility Requirements

the basic vehicle. This type of vehicle can be considered to have variable geometry as compared to the fixed-geometry entry vehicles.

**4.2.1 FIXED GEOMETRY.** For the designer of a fixed-geometry re-entry vehicle it becomes necessary to determine to what extent he can compromise the configuration trades and still have a vehicle that can perform an acceptable landing. Criteria for judgement of the capability of the vehicle to perform an acceptable piloted landing have been developed through analysis and pilot opinion to allow the designer to assess his design, once he has determined its low-speed, lift-drag polar. The criteria are based primarily in altitude lost in flare and time remaining between the end of flare and touchdown. It has been shown that the value of maximum  $L/D$  and the ratio of touchdown  $C_L/C_{L(L/D)_{\max}}$  can be used to check the landing acceptability of a vehicle.

A consideration must be given to the aerodynamic trades on configuration details for fixed-geometry vehicles that must operate in a flight regime that extends from orbital speeds to sub-sonic landing speeds. For the entire regime, it is essential that the vehicle have good handling qualities beyond the intended operation. In general, this leads to requirements for static stability and high-control effectiveness to augment those regimes where damping is practically nonexistent.

In the evolution of the vehicle design, achievement of adequate performance capability is equal in importance to handling qualities. Strictly speaking, the landing phase commences at deorbit.

Fixed-geometry vehicles whose characteristics result in large hypersonic  $L/D$ 's (1.0, 1.5, 2.0) usually have relatively small subsonic  $L/D$ 's (3.0, 3.5, 4.0). The trend of hypersonic  $L/D$  with wing sweepback angle, when the leading edge radius is varied to give constant leading-edge temperature, is an increase in  $(L/D)_{\max}$  with increasing sweepback to approximately 80 degrees. For a subsonic wing the  $(L/D)_{\max}$  decreases with increasing sweepback.

**4.2.1.1 Wing Effects.** The effects of wing section on elevator effectiveness at hypersonic speed, subsonic  $(L/D)_{\max}$ , and maximum usable  $C_L$ , as limited by pitchup at subsonic speeds, are shown in Figure 14. Cambered or symmetric subsonic type airfoils show a loss in effectiveness at hypersonic speeds from the basic flat plate, due to the adverse expansion that takes place around the curved airfoil. Improvements are made in subsonic  $(L/D)_{\max}$  for the cambered airfoils over the flat plate airfoils due to smaller leading-edge separation drag. The symmetrical section shows an improvement in subsonic  $(L/D)_{\max}$  over the cambered section. For equal stability, the symmetrical section requires less elevator deflection to trim, since the cambered section has a  $-C_{m_0}$  and costs more in trim drag.

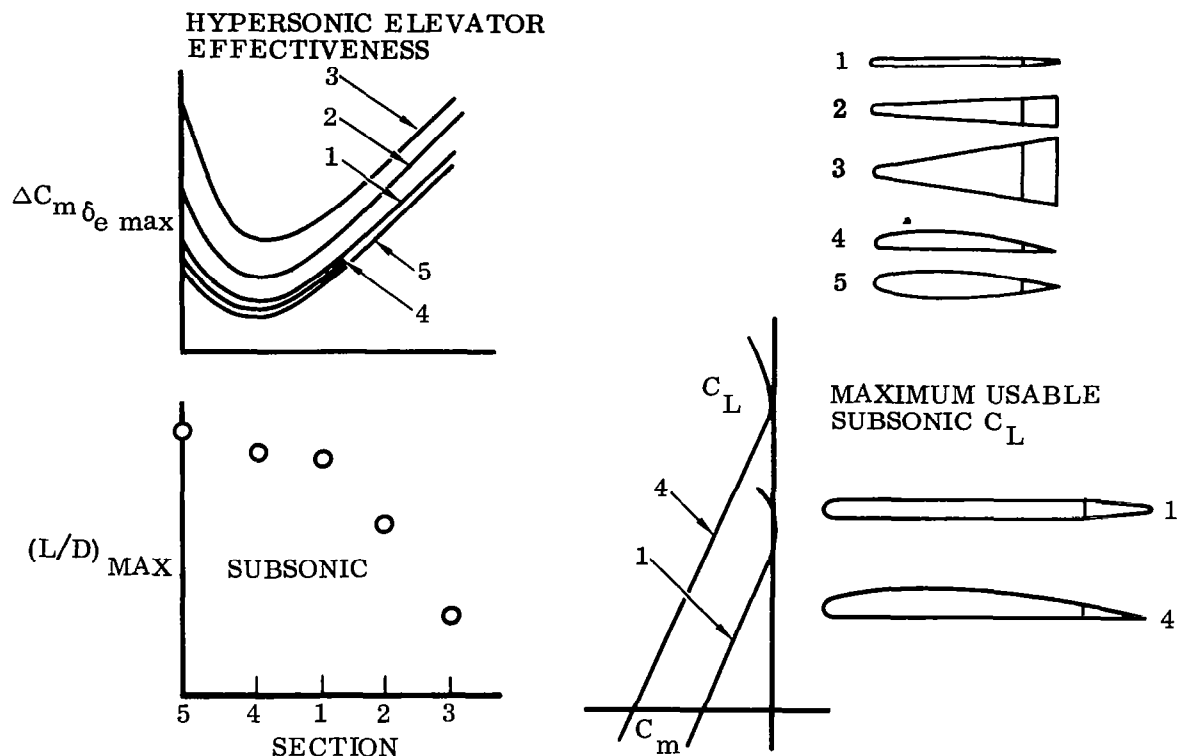


Figure 14. Effect of Wing Section

**4.2.1.2 Fin Toe-In Effects.** The trades between directional stability at hypersonic and transonic speeds, and hypersonic and subsonic  $(L/D)_{\max}$ , are shown in Figure 15. The higher stability at hypersonic speeds of the greater toe-in is due to the fact that the greater the toe-in (up to a point) of the fin, the greater the rate of change of pressure with side-slip. Losses in both hypersonic and subsonic  $(L/D)_{\max}$  are experienced with increased toe-in due to increased initial pressures and deflection angle at hypersonic speeds and due to separation off the inner surface at subsonic speeds. At transonic speeds the losses in directional stability with increased toe-in are due to earlier and greater losses in the slope of the lift curve of the fin. An additional penalty of toe-in is the high hinge moment acting at the rudder at supersonic speeds.

**4.2.1.3 Body Aft-End.** The effect of body aft-end closure on hypersonic and subsonic  $(L/D)_{\max}$  is shown in Figure 16. There is no change in hypersonic  $(L/D)_{\max}$ , but subsonic  $(L/D)_{\max}$  improves as the base area of the configuration is decreased. Subsonic directional stability is reduced by body aft-end closure.

**4.2.1.4 Fin Sweep.** The effect of fin sweepback angle on subsonic directional stability is shown in Figure 17. The directional stability decreases with increasing sweepback angle due to decreases in the slope of the lift curve.



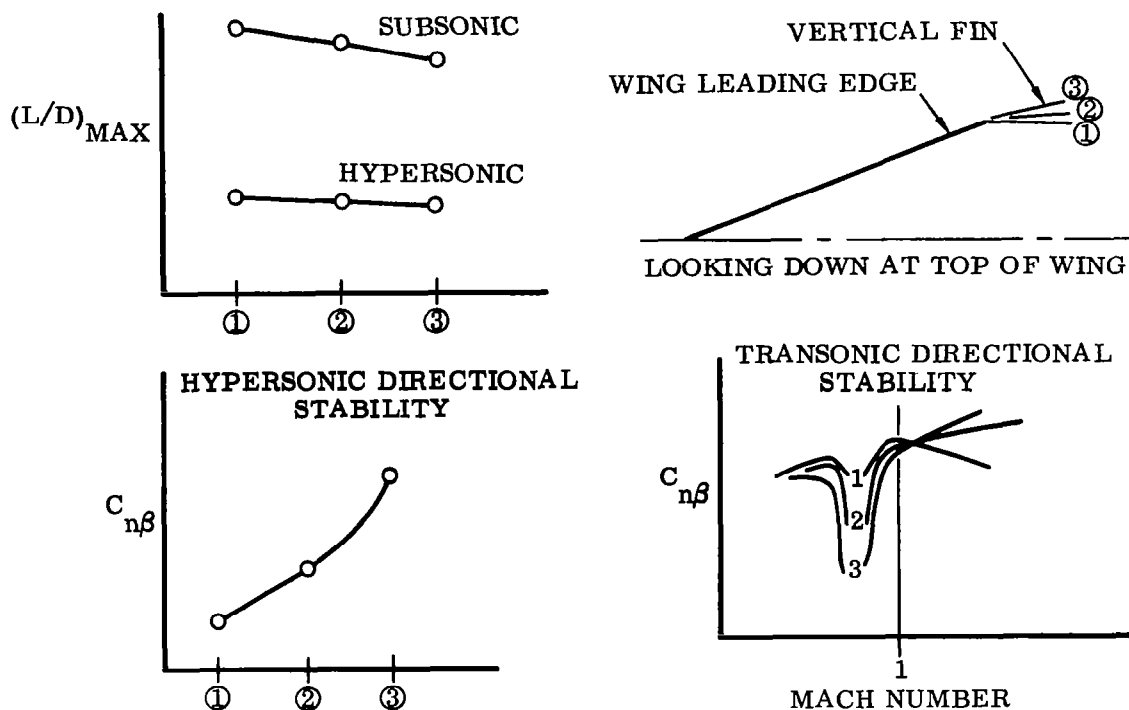


Figure 15. Effect of Fin Toe-In

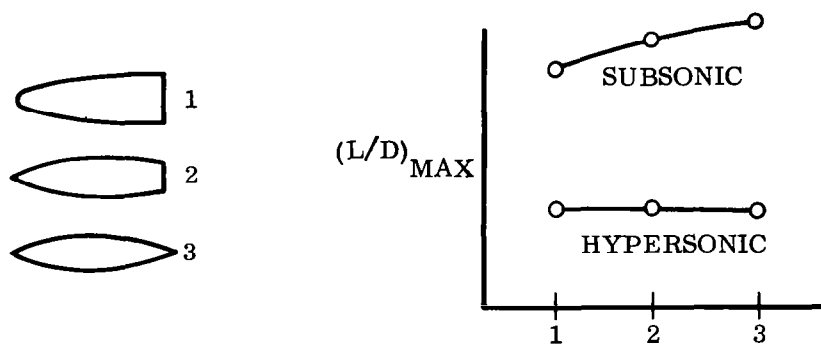


Figure 16. Effect of Body Aft End

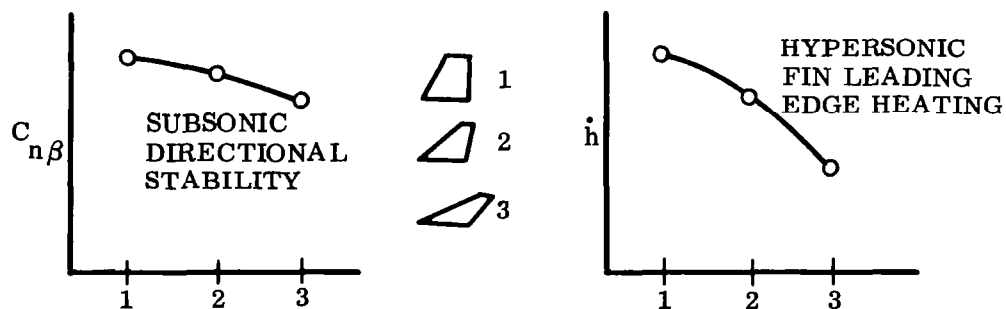


Figure 17. Effect of Fin Sweep

To satisfactorily achieve the proper balance between the two flight regimes, the designer must ensure that the configuration can be flown successfully through the transonic regime.

**4.2.1.5 Landing Criteria.** The landing technique to be considered is the high energy approach landing (Reference 7). A brief description of this approach and landing, consisting of six separate phases, is presented below (see Figure 18):

- a. The first phase is pilot guidance of the vehicle to a high-key position near the landing site after deorbit and re-entry through information obtained by an inertial navigation system enroute and a radar voice system aid within a few hundred miles of the landing site.
- b. The second and ensuing phases are shown in Figure 18. This phase, from high-key through mid-key and low-key to the final approach leg, is used by the pilot to check his position and speed against a predetermined schedule, so that he enters the approach leg at the desired speed, attitude and heading.
- c. In the third phase, the pilot maintains a steady-state glide at constant equivalent airspeed, aiming at a point short of the runway.
- d. At a predetermined altitude, the pilot starts an approximately constant normal acceleration to arrest the vehicle rate-of-sink. This fourth phase ends at a small altitude above the ground and the normal acceleration is reduced to near one g.

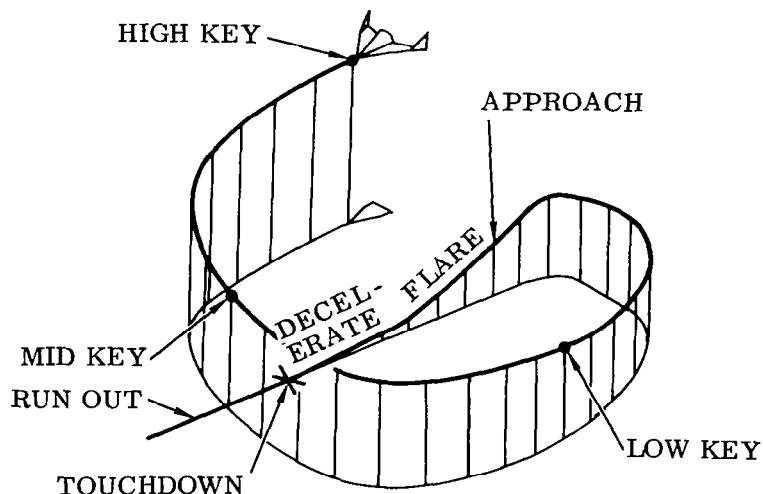


Figure 18. Landing Phases

- e. Phase five is a deceleration to touchdown. After the flare the pilot continues to reduce speed as he gradually reduces his altitude along a small flight path angle until ground contact is made. This phase is sometimes called float time.
- f. The last phase is the runout phase during which the vehicle's speed is completely arrested and the pilot performs ground steering to remain on the runway.

In the second phase of the landing maneuver speed brakes serve their greatest usefulness. The pilot will exercise both bank maneuver and speed modulation to successively reduce errors checked at each key, thus minimizing his error when entering the final approach leg. It is important that speed-brake deployment does not alter longitudinal trim. It is highly desirable that this phase take place after the transonic aerodynamic center shift has taken place.

The third, fourth and fifth phases of landing are interrelated. Figure 19 illustrates these phases and the associated points of operation on a lift-drag polar. The most important elements are all those associated with the pilot's approach, rate-of-sink in the approach, flare altitude, flare load factor, and time remaining after flare and touchdown speed.

Since the pilot aims for a point short of the runway it is considered advisable to have a flight path angle that is high enough so that the apparent motion of the aiming point is relatively insensitive to changes in flight path angle. Consequently, the flight path angle should be at least 10 to 15 degrees. An angle higher than 45° would probably be quite uncomfortable to the pilot.

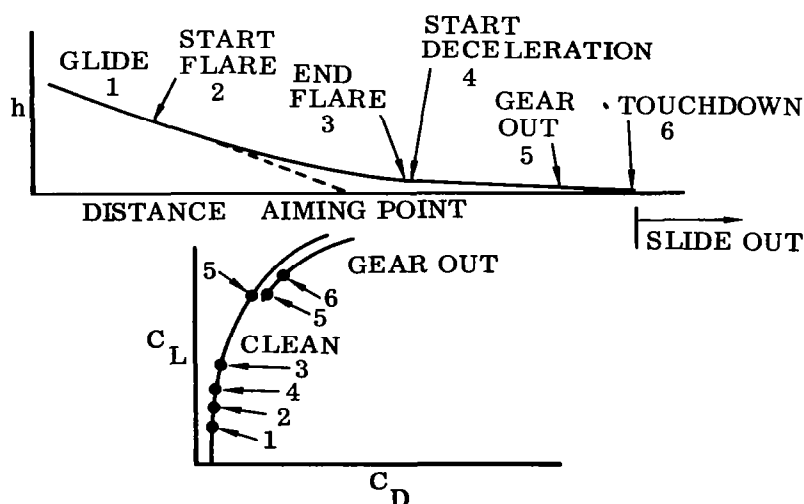


Figure 19. Landing Profile and Polar

The speed of the vehicles should be high enough to perform the flare maneuver on the front side of the L/D curve [i. e. before  $(L/D)_{\max}$ ]. It has been demonstrated that if the ratio of touchdown lift coefficient to lift coefficient at maximum L/D is 1.3 then the pilot has the ability to flare on the front side of the L/D curve.

Pilots prefer to maintain a margin of excess speed throughout the landing maneuver to improve the control characteristics. However, there is a point at which increased speed in the landing maneuver becomes extremely detrimental to the landing performance characteristics. Maximum touchdown speed is associated with ability to handle the slide-out (runout). The higher the slide-out the more demanding is the requirement for surface smoothness.

**4.2.1.6 Landing Analysis.** Landing analyses have been made and are documented in Reference 8. These analyses show that for parabolic polar assumptions, the prime landing performance parameters — altitude consumed during flare and deceleration time — can be determined as a function of  $(L/D)_{\max}$  and the ratio of touchdown  $C_L/(C_L)_{L/D_{\max}}$

Since the altitude consumed during flare ( $\Delta h$ ) and deceleration time ( $\Delta t$ ) are the prime parameters used in evaluating the landing characteristics of an entry vehicle, the following section presents a brief derivation of the equation expressing these parameters as functions of  $(L/D)$  and  $C_L$ .

The basic equations of motion of a point mass are\*:

$$L - mV\dot{\gamma} - mgc\gamma = 0 \quad (4-1)$$

$$D + m\dot{V} + mgs\gamma = 0 \quad (4-2)$$

$$\Delta h = \frac{V}{\dot{\gamma}} s\gamma d\gamma \approx \frac{V_{\text{avg}}^2 s\gamma d\gamma}{g \left[ \left( \frac{L}{W} \right)_{\text{avg}} - c \left( \frac{\gamma g}{2} \right) \right]} \quad (4-3)$$

$$\gamma_g = \gamma_{\text{glide}}$$

then

$$\Delta h = \frac{V_{\text{avg}}^2 (1 - c\gamma_g)}{g \left[ \left( \frac{L}{W} \right)_{\text{avg}} - c \left( \frac{\gamma_g}{2} \right) \right]} \quad (4-4)$$

---

\*The symbols s and c refer to sine and cosine in Equations 4-1 through 4-12.

assume

$$V_{avg}^2 = \frac{1}{2} \left[ V_{glide}^2 + V_{end\ of\ glide}^2 \right] \quad (4-5)$$

$$V_{end\ of\ flare}^2 = \frac{2 \cdot W}{\rho A C_{L_{end\ of\ flare}}} g \left[ \left( \frac{L}{W} \right)_{avg} - c \left( \frac{\gamma_g}{2} \right) \right]$$

$$\Delta h = \frac{\frac{W}{A C_{L_{glide}}} \left[ c \gamma_g + \frac{C_{L_{glide}}}{C_{L_{end\ of\ flare}}} \right] (1 - c \gamma_g)}{\rho_{avg} g \left[ \left( \frac{L}{W} \right)_{avg} - c \left( \frac{\gamma_g}{2} \right) \right]} \quad (4-6)$$

The deceleration time then becomes:

$$\dot{V} = g \left[ \frac{1}{L/D} + s \gamma \right] \quad (4-7)$$

$$L \approx W$$

If we further assume that  $\dot{V}$  is constant

$$\Delta t = \frac{-\Delta V}{g \left[ \frac{1}{L/D} + s \gamma \right]} \quad (4-8)$$

$$-\Delta V = V_{end\ of\ flare} - V_{touchdown} \quad (4-9)$$

for

$$V = \sqrt{\frac{2W}{\rho A C_{L}}} \quad (4-10)$$

then

$$\Delta V = V_{touchdown} \left[ \sqrt{\frac{C_{L_{touchdown}}}{C_{L_{end\ of\ flare}}} - 1} \right] \quad (4-11)$$

and

$$\Delta t = \frac{V_{\text{touchdown}} \left[ \sqrt{\frac{C_{L_{\text{touchdown}}}}{C_{L_{\text{end of flare}}}}} - 1 \right]}{g \left[ \frac{1}{L/D} \right] + s\gamma} \quad (4-12)$$

Families of curves may be arrived at which specify  $\Delta h$  and  $\Delta t$  as functions of  $(L/D)_{\text{max}}$  and touchdown  $C_L/(C_L)_{L/D_{\text{max}}}$ . Once acceptable landing values  $\Delta h$  and  $\Delta t$

are established, the capability of any vehicle to perform an acceptable high energy approach can be checked.

For a given vehicle, it is possible to trade off the altitude consumed during flare and the time remaining after flare to touchdown with a given flare load factor by varying the glide angle during approach. A comparison of the trades for a steep approach and a shallow approach for a vehicle is shown in Figure 20. Performance variation as affected by maximum  $L/D$  is shown in Figure 21 for maximum  $L/D$ 's of 3, 4, and 5 for a touchdown  $C_L/(C_L)_{L/D_{\text{max}}}$  of 1.6. Noted improvements are gained by going to a higher  $L/D_{\text{max}}$ .

Acceptable, marginal and unsatisfactory regions for landing are defined (Figure 22) in terms of maximum  $L/D$  and touchdown  $C_L/(C_L)_{L/D_{\text{max}}}$ .

The approach characteristics of vehicles operating along the two upper boundary lines in Figure 22 as affected by wing loading and touchdown velocity are shown in Figure 23.

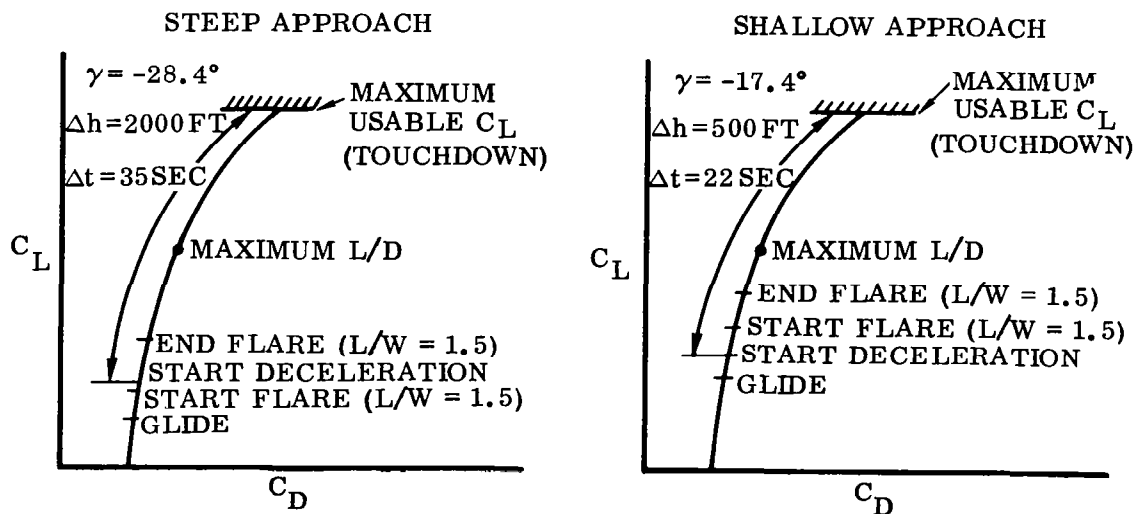


Figure 20. Approach Comparison for a Typical Vehicle

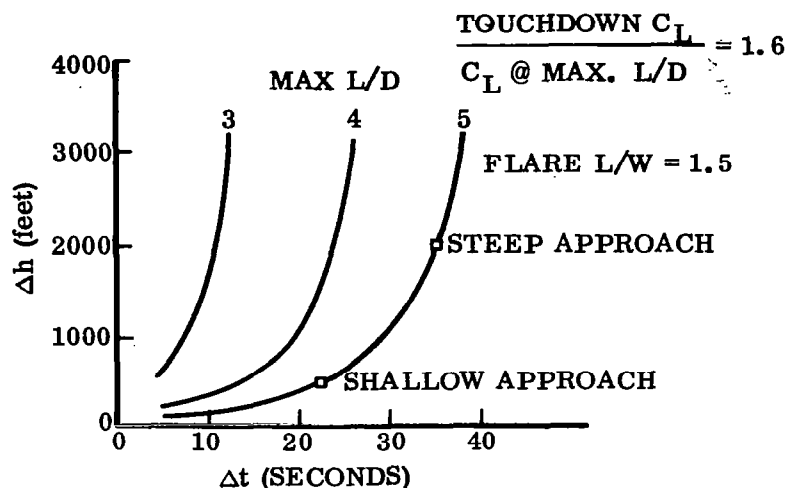


Figure 21. Performance Variation with Approach Angle and Maximum L/D

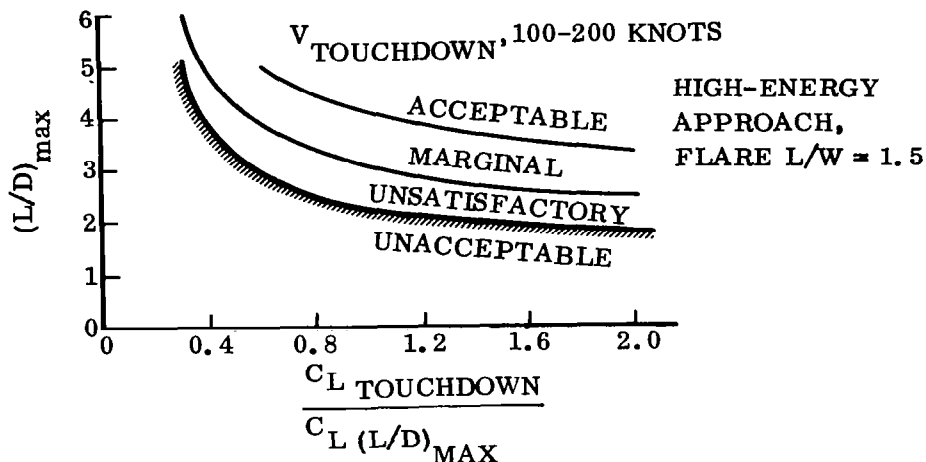
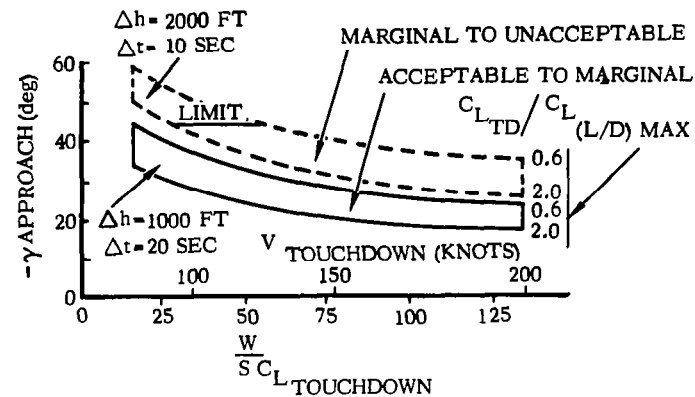


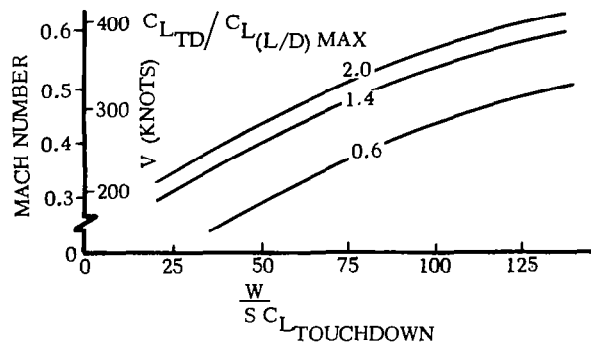
Figure 22. Landing Performance Criteria

Since improvements in landing characteristics can be obtained by increasing the touchdown  $C_L$  efforts should be made in providing longitudinal static stability up to  $C_{L_{max}}$ . Configurations with high subsonic L/D have been conceived which have longitudinal stability boundaries that are at  $C_L$ 's well below  $C_{L_{max}}$ . Looking at the maximum subsonic L/D of a vehicle is a short-sided way of evaluating the landing characteristics of the vehicle.

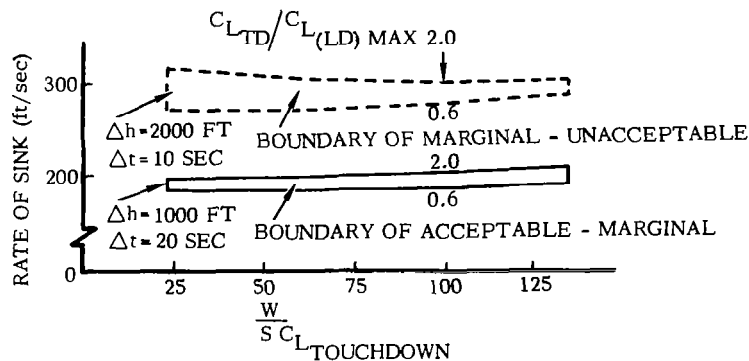
Gusts constitute the major disturbance with which a horizontal landing vehicle must contend. Consider the  $\Delta\alpha$  due to gust for one-percent gust condition (30 fps sharp-edge gust) as shown in Figure 24. To indicate the effects of gust on the behavior of the re-entry vehicle near touchdown, let us assume three hypothetical low-aspect ratio, fixed-geometry re-entry vehicles. In general, low-aspect ratio re-entry vehicles have a low slope of the lift curve. If we assume that  $C_L$  is 0.04 per degree and that touchdown  $C_L$  varies with selected touchdown speeds so that it is 1.0 at 50 knots,



a. Approach Angle



b. Approach Mach Number



c. Approach Rate of Sink

Figure 23. Approach Characteristics as Determined by Wing Loading and Touchdown Velocity



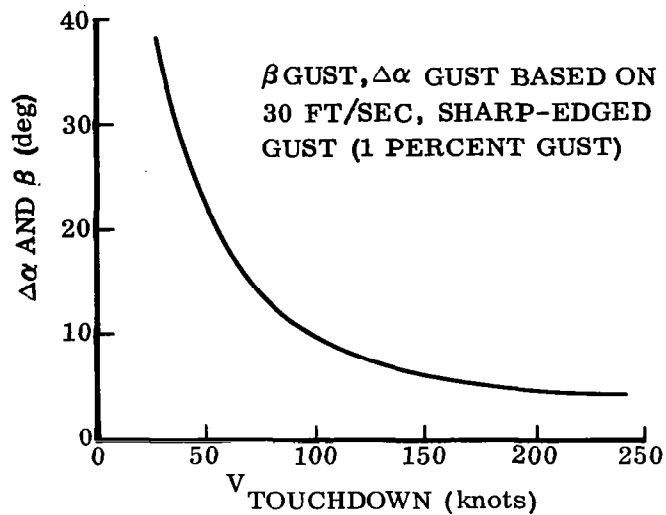


Figure 24. Gust-Induced Angle Changes

0.75 at 125 knots, and 0.5 at 200 knots, the values for corresponding wing loading and resultant acceleration when each vehicle is subjected to a one-percent vertical gust are:

$V_{TD}$ (kts)	$q$ (psf)	$W/S$ (psf)	$\alpha_{TD}$	$\Delta\alpha$	$\Delta(L/W)\Delta\alpha$	$\Delta(L/W)q$	NET ( $\Delta L/W$ )
50	8.5	8.5	$25^\circ$	$\pm 23^\circ$	$\pm 0.92$	+0.2	+1.12 - 0.72
125	55	40	$18.7^\circ$	$\pm 8^\circ$	$\pm 0.45$	Neg.	$\pm 45$
200	136	68	$12.5^\circ$	$\pm 0.5^\circ$	$\pm 0.40$	Neg.	$\pm 0.40$

The structure of gusts consists of a gradient buildup over a few seconds, maintenance of peak values for a few seconds and then a cessation. A good approximation of a one-percent gust condition can be made by applying a gust instantaneously and holding it constant for one second. This approximation allows us to make a simple examination of velocities and displacements of the three hypothetical vehicles. The numerical values under the conditions assumed are:

$V_{TD}$ (kts)	W/S (psf)	$\Delta V_V$ (fps)	$\Delta h$ (feet)
50	8.5	+35, -23	+18, -12
125	40	$\pm 14$	$\pm 7$
200	68	$\pm 12$	$\pm 6.5$

Under the assumed conditions of analysis, it is apparent that the direct effects of gust on changes of acceleration, vertical velocity and altitude are most severe for lightly loaded, low-touchdown velocity vehicles. These effects are considerably reduced as the wing loadings are raised to values above 40 psf. Also, the allowable touchdown  $C_L$  must include a reserve in  $\Delta\alpha$  below angles of attack for the onset of directional or longitudinal instability so that the vehicle is not upset by the gust condition.

Since the landing of a fixed-geometry re-entry vehicle depends upon a high energy approach, the visibility of the pilot to perform the landing site acquisition and flare must be extremely good. The curves on Figure 25 show the minimum cloud ceiling requirement to provide pilot visibility at high key, low key, 15 seconds before flare and flare altitude. These curves are based on flight data for the X-15, F-100, and the T-33 in the power-off, high energy landing approach technique. Each line assumes that the pilot has been guided to that condition by radar and voice contact.

Assuming accurate placement of the vehicle at high key and a vehicle maximum L/D greater than 4, present Precision Controlled Radar capability can direct the pilot to his low-key position with sufficient accuracy to allow him to correct all remaining dispersions during his final turn to the approach. For operation in ceilings below this minimum, PCR installations would have to be modified to accommodate the steep glide slopes associated with the specific re-entry vehicle design. If the pilot is to perform any useful function in the approach and touchdown, the last time he can be assumed to take over visually is 15 seconds prior to flare. Consequently, the operational weather restrictions versus  $(L/D)_{max}$  for piloted landing is defined by Line A. Operation in weather conditions below line A will require a completely automatic landing system for the unpowered vehicle. To have piloted capability operating at very low ceiling (200 - 300 ft) would require  $(L/D)_{max} \approx 12$ . This capability for present concepts in hypersonic configurations would require the use of on-board propulsion or foldout wing (variable geometry) capability.

The criticality of providing good visibility for reference and good handling qualities is brought out by a recent accident involving NASA's fixed-geometry M2-F2 research re-entry vehicle. The cause of the accident was an unusual combination of circumstances, including disorientation and distraction of the pilot.

The research flight was normal through two 90-degree turns from the downwind leg to the base leg and from the base leg to the final leg. Due to a variable crosswind

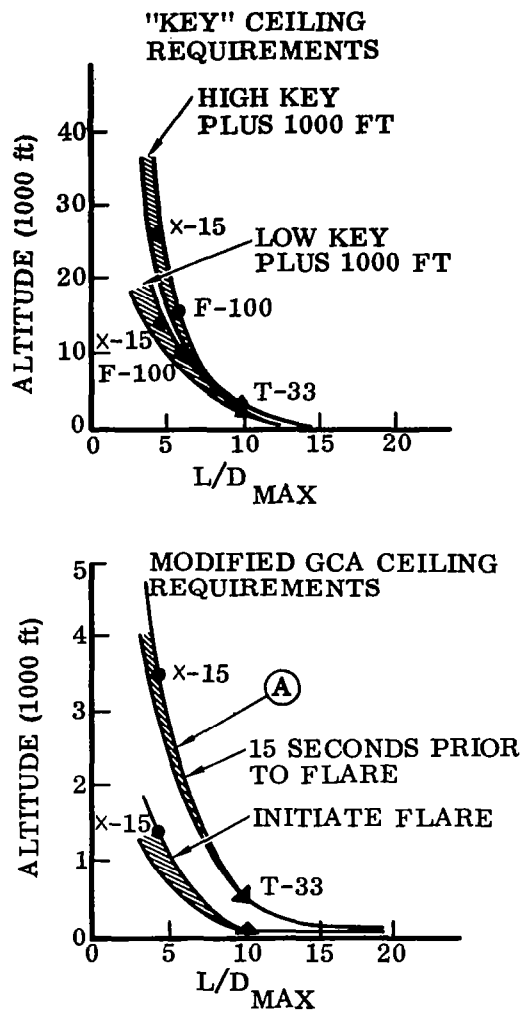


Figure 25. Demonstrated Ceiling Requirements for Unpowered Landings

condition the pilot planned to make an S-turn on the final approach, with a slight left turn followed by a right turn to angle across the runway outline painted on the dry lake bed landing site.

In coming out of the second left turn, leveling from a banked condition, a lateral oscillation developed and quickly increased in amplitude. Roll rate of 200 deg/sec and bank angle of 140 degrees were reached. It took 11 seconds to bring the vehicle under control.

The M2-F2 is most prone to lateral oscillatory motion, pilot or gust induced, at low angles of attack. This can occur if the pilot pushes forward on the stick to gain speed in the preflare maneuver. Neither the rudder nor the ailerons are effective in damping the oscillation; and pulling back on the stick to increase angle of attack is the standard recovery procedure.

The temporary loss of lateral control by the pilot while in the landing approach resulted in a change in the landing heading and area, which caused the pilot to be disoriented in the final phase of the landing. By the time lateral control was regained, the heading to which the pilot was committed left him without the runway-type markings normally used for both landing directions and visual height cues, and the vehicle was placed on a flight path that caused the pilot to be disturbed by the possibility of a collision with rescue aircraft in the area.

The unusual disturbances caused the pilot to initiate his flare maneuver at a lower altitude than normal. The vehicle contacted the ground just as the vertical velocity was arrested but before the landing gear was deployed. After bouncing, sliding and rolling over several times the vehicle came to rest.

This accident also pointed out the need to ease the landing task for the pilot of fixed-geometry re-entry vehicles so as to give greater allowance for unusual events.

4.2.2 VARIABLE GEOMETRY. Recent spacecraft designs have encompassed hypersonic (L/D)'s from about 1 to greater than 3, all with horizontal ground landing. Results have indicated that the use of variable geometry features can provide useful flexibility and significant aerodynamic performance enhancement over the operating regime. Variable geometry will not unduly compromise the hypersonic performance of good aerodynamic design while providing favorable low-speed and tangential landing characteristics.

Variable-geometry spacecraft have been designed with subsonic maximum (L/D)'s from 7 to 16. The method for evaluating landing characteristics of horizontal landing spacecraft that was presented in the fixed-geometry section of this report is directly applicable to variable geometry vehicles.

Wing deployment transients might place severe requirements on the vehicle control system. Because the equations of motion which best model this motion are highly nonlinear (inertia coupling and aerodynamic data as function of wing position), it is almost impossible to analyze the motion without the aid of a multi-degree-of-freedom simulation. However, a qualitative approach to the problem can be gained by looking at several possible basic types of wing deployment methods.

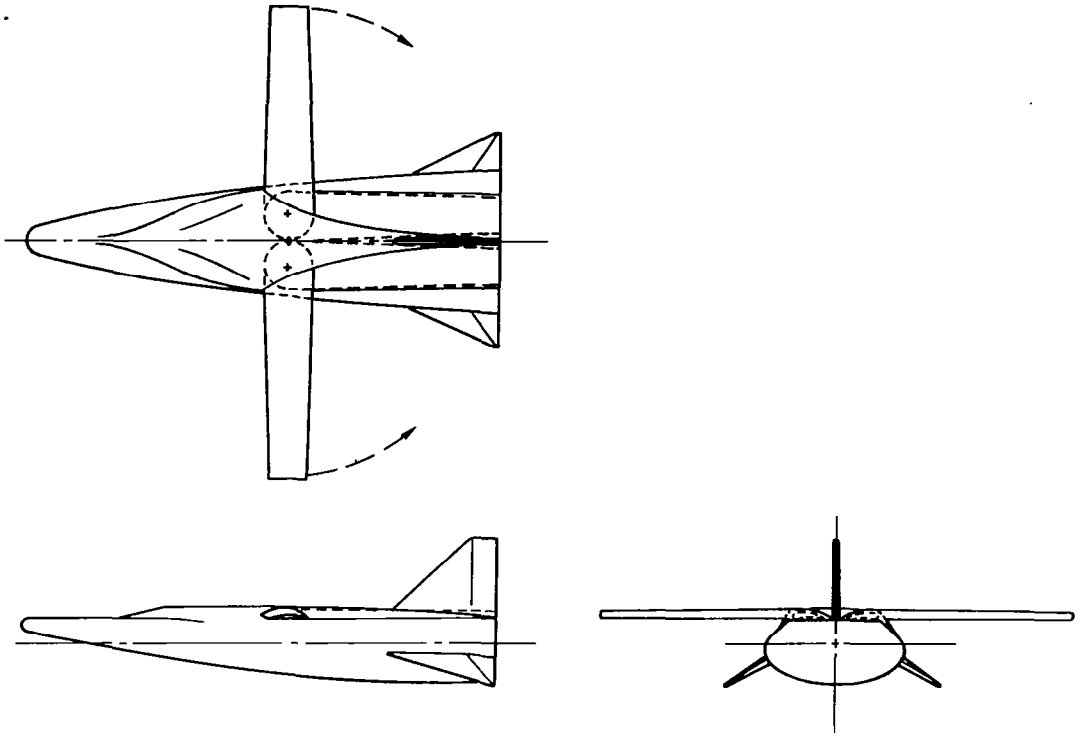
**4.2.2.1 Switch-Blade.** Figure 26 shows a nominal design for a switch-blade wing deployment scheme. At subsonic speeds the major portion of the lift is carried by the wings with a resulting low angle of attack during landing. The major control system problem area is aerodynamic center-of-pressure changes as function of wing position. If the wing is deployed at subsonic speeds the problem and solution is similar to that which was encountered in the F-111 program. However, if the wing deployment occurs at supersonic speeds then changes in the lateral aerodynamic characteristics can produce unfavorable Dutch-roll handling qualities.

**4.2.2.2 Fold-Out.** Figure 27 shows a nominal design for a fold-out wing deployment scheme. The wing for this configuration has a thin airfoil section readily storable into the side of the body. Because of the thin airfoil section, leading and trailing edge devices (flaps and slats) may be required to obtain the desirable  $C_L$  at landing. Deployment of the wing during the transonic speed region may produce severe lateral handling problems because of the large dihedral effects.

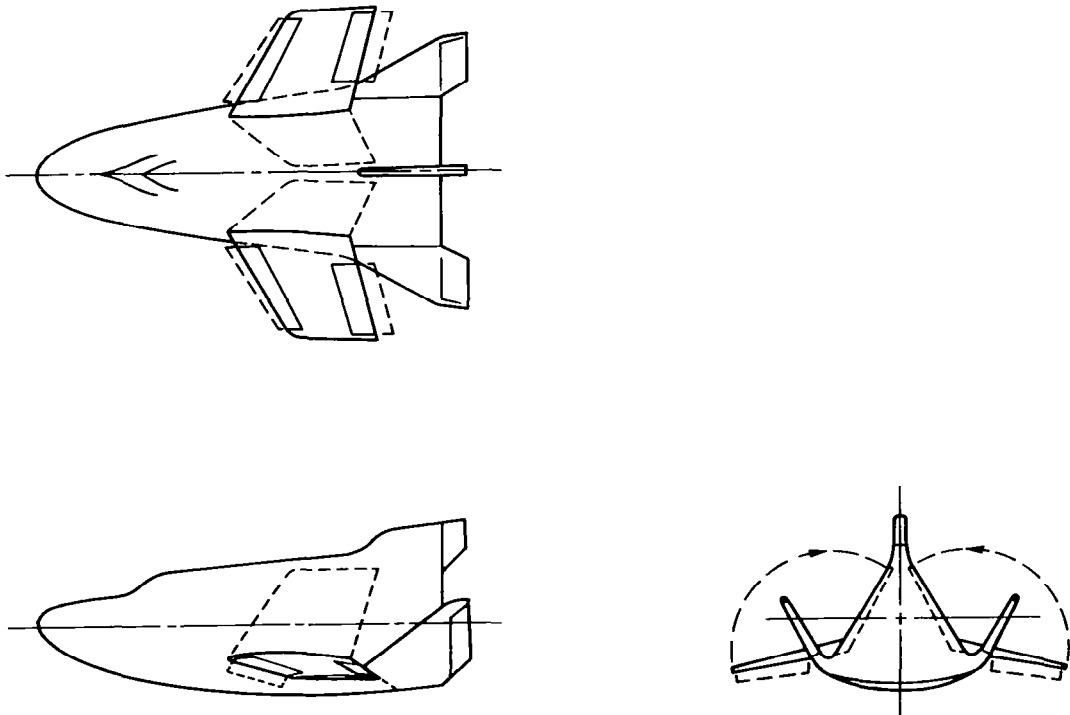
As dihedral effect is increased negatively by increasing dihedral angle, the spiral mode becomes stable, while the Dutch-roll damping weakens and then goes unstable. A good level of Dutch-roll stability is always important. It is difficult to overcome by control manipulation a poorly damped oscillation of moderate frequency while it is continually excited by turbulence. At low speeds, where accurate path control may be essential, good Dutch-roll stability is vital.

**4.2.2.3 Single Pivot.** Figure 28 shows a nominal design for a single pivot, two-position skewed wing. A rapid wing deployment sequence is considered essential to reduce transient effects. This type of wing would only be deployed at subsonic speeds. During the deployment, aerodynamic coupling of all three axes will occur, which might result in extreme control system requirements.

For vehicles of this type the flow field of the body interacts with the wing in such a way as to modify the local angle of attack. Consider the cross-flow component of the stream of magnitude  $V\beta$  and the flow pattern which it produces about the body, Figure 29. The body induces vertical velocities which when combined with the mainstream velocity alter the local angle of attack. When the wing is at the top of the fuselage the lift on one wing is increased while on the other wing there is a reduction of lift. For a single wing pivot vehicle this angle of attack distribution will produce rolling, yawing, and pitching moments.



**Figure 26. Fineness Ratio 6 Elliptic Lifting Body Configuration Having Variable Position, Switch-Blade Wings**



**Figure 27. Low Fineness Ratio Lifting Body Configuration Having Foldout, Variable Geometry Wings**

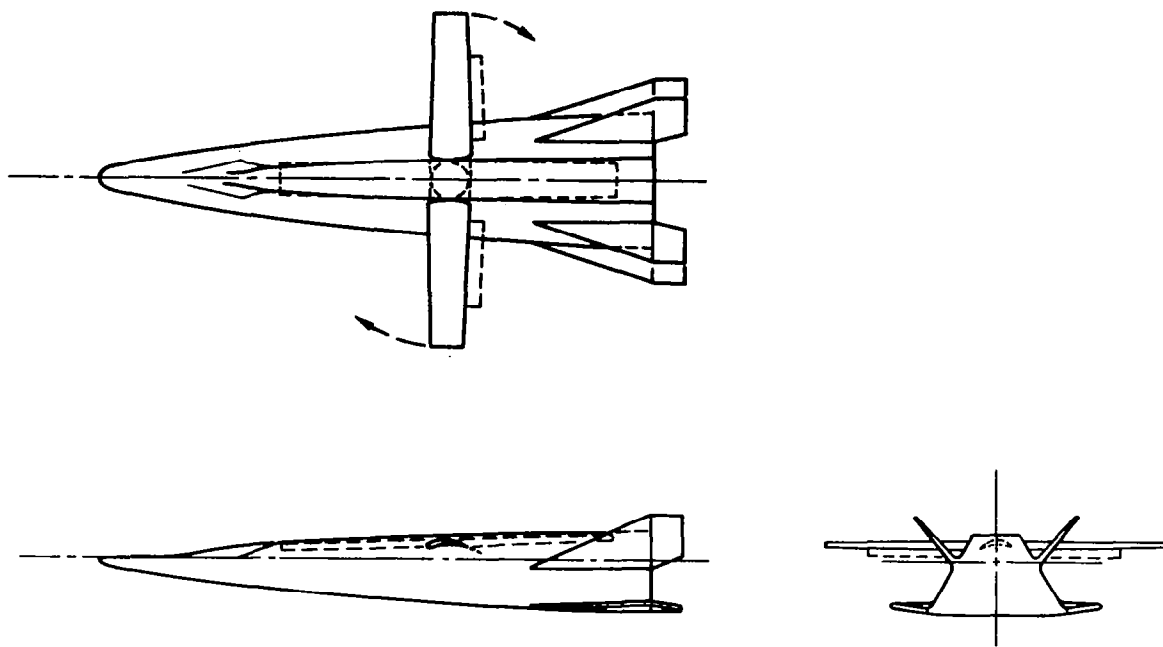


Figure 28. High Fineness Ratio Trapezoidal Lifting Body Configuration Having Two-Position, Single Pivot Skewed Wing

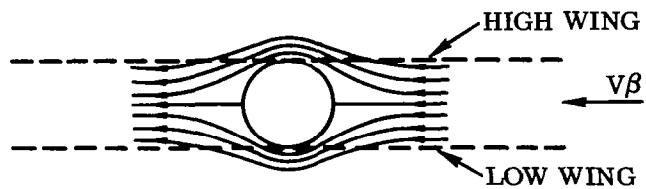


Figure 29. Influence of Body on  $C_{l\beta}$

### 4.3 POWERED LANDING SPACECRAFT

As the designer looks ahead toward greater versatility in the final descent and landing operation, he naturally turns attention to powered descent modes. Two such modes being examined are the powered-rotor and sustained-propulsive-lift system. The former can draw on a substantial background of helicopter experience, and the latter on rapidly advancing technology in reaction controls, the LEM and VTOL systems. The attraction of these modes derives from their ability to approach the zero-vertical, zero-horizontal landing velocity and their uniqueness in providing a late decision-reversal capability near the touchdown point, and brief decision-holds (hover). These factors combine to impose the least stringent requirements of all the landing modes on land site surfaces roughness, obstacles, precise touchdown point within the landing area, etc.

Powered modes pose several operational questions that are being explored in current studies. For the stowed rotor, operation between initial deployment of the rotor and application of power presents unresolved problems in sequencing and control. In fact, maneuver and control can be considered a general area of neglect in past studies of rotor descent modes, powered or autorotative. The problem for propulsive-lift systems presents no less a challenge. Can the transition from aerodynamic flight to the propulsive lift mode be made directly or might it be done better with indirect transition such as a brief period of rapid drogue or chute descent?

**4.3.1 PROPULSIVE LIFT.** Three possible propulsive-lift configurations are presented in Figure 30. The most promising and the one studied in detail is the Propulsive Lift and Maneuvering Entry (PLAME) vehicle shown in Figure 31.

The PLAME concept is as follows: The vehicle performs a conventional maneuvering lifting entry, and when the velocity has been reduced to about Mach 2.5, a drogue parachute is deployed which stabilizes the vehicle through the transonic speed regime, thus eliminating aerodynamic problems in this and the subsonic regime. A second drogue is deployed subsonically, slowing the vehicle for deployment of the main parachute at about 12,000 feet altitude. Lift engines on the vehicle are then started but are left idle (except for checkout) while descending on the main parachutes to a very low altitude. Power is applied to the lift engines, the parachute is jettisoned, and the vehicle now operates as a VTOL aircraft to accomplish a certain amount of ranging to a suitable touchdown point, where it lands vertically.

Work performed at Langley Research Center using a variable stability helicopter and work performed at the NASA Flight Research Center using the LLRV (Lunar Landing Research Vehicle) in free flight tests has indicated a substantial advantage in using an on-off control system for hovering control as compared to using a proportional system. With an on-off system, the control power requirements for satisfactory hovering handling qualities are reduced to some 30% of the values thought



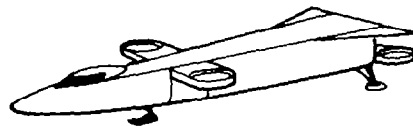
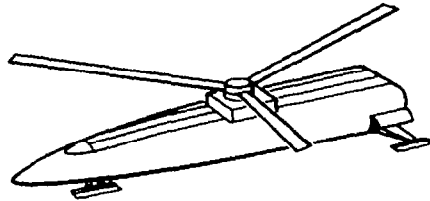
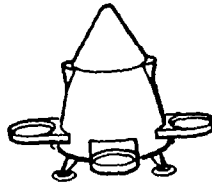


Figure 30. Propulsive Lift Vehicles

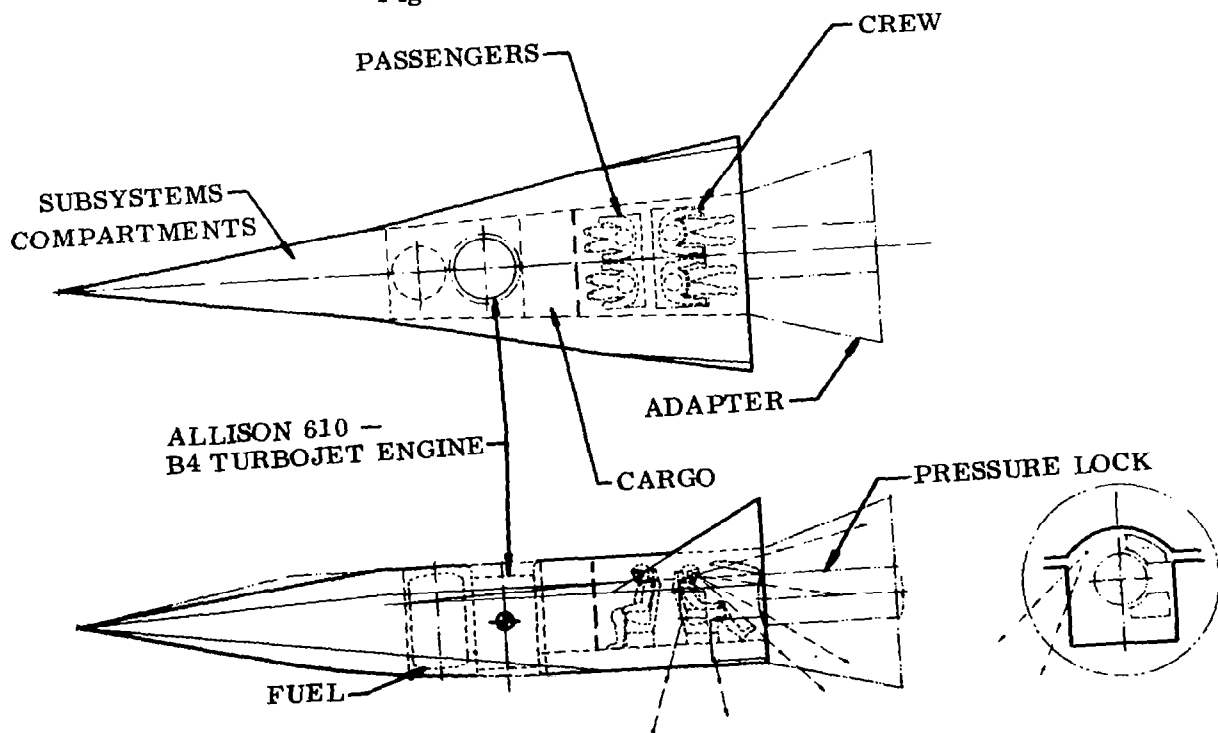


Figure 31. PLAME Vehicle

necessary heretofore. Typical requirements for both systems for hover vehicles are shown in Figure 32. As shown, the on-off system has a closed satisfactory area, wherein the handling qualities actually deteriorate if the control power is increased.

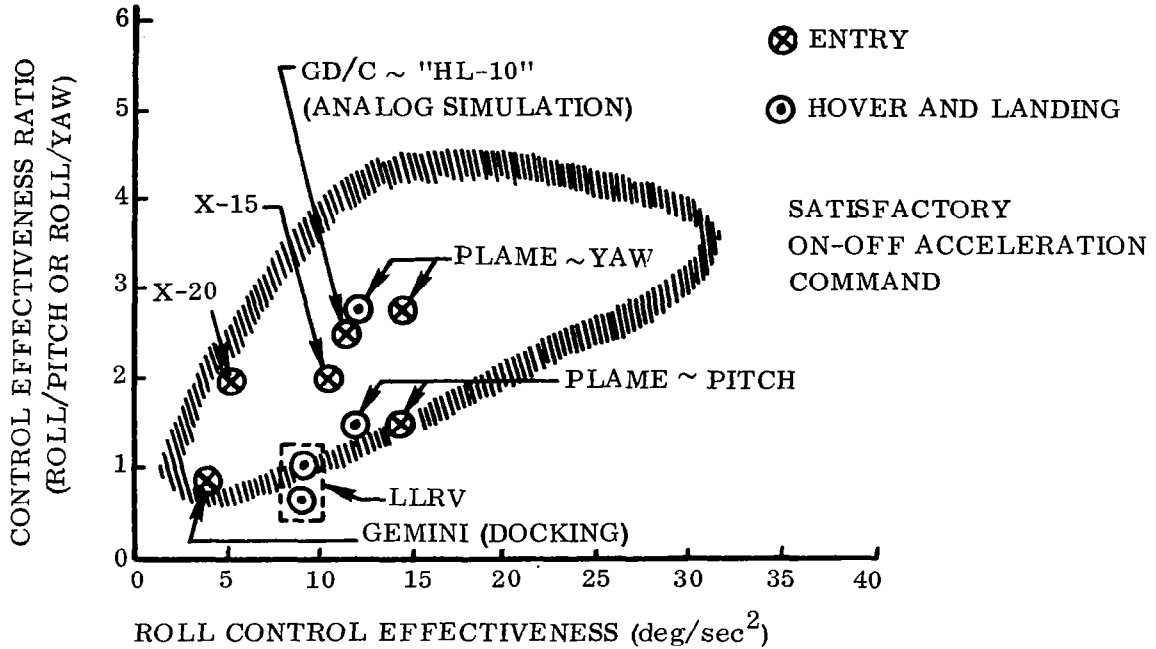


Figure 32. Typical System Requirements

A significant amount of control power is needed to trim-out the pitching moments produced by the engine inlets and exhaust. The inlet moment can be approximated by a momentum balance for the air flow and by assuming that the resultant force acts one inlet diameter above the inlet. This leads to the equations:

$$M_{\text{pitch}} = \frac{\dot{W}}{g} \ell_{\epsilon} (U - \ell_{\epsilon} Q)$$

where

$M_{\text{pitch}}$  = the pitching moment

$\dot{W}$  = the air weight flow rate

$g$  = 32.2 ft/sec<sup>2</sup>

$U$  = the forward velocity of the vehicle

$Q$  = the vehicle pitching velocity

$\ell_{\epsilon}$  = the effective moment arm (one engine diameter)

Similarly the pitching moment due to engine exhaust can be obtained, and a good approximation is:

$$M_{\text{pitch}} = KU^2$$

where K is a function of the lift engine size.

To eliminate gyroscopic effects and those from other engine considerations, two lift fan engines have been considered in most designs. The dual engine concept can be used to alleviate the problem of large engine moments. With two engines, differential thrust can be used along with the on-off control system. Then, the total control moment available as a function of command might be as shown in Figure 33. Studies have shown that the maximum forward velocity that can be attainable by the PLAME vehicle is limited by the control power available.

The main parachute has a single-point attachment in order to simplify the parachute jettison; since the attach point is aft of the vehicle center of gravity (see Figure 34), the vehicle is at a trim pitch attitude. A parachute jettison technique has been developed beginning with the vehicle in a steady-state rate of descent. As the main engines are started and the thrust increases, the parachute moment tends to trim the vehicle at successively smaller pitch angles and the vehicle picks up

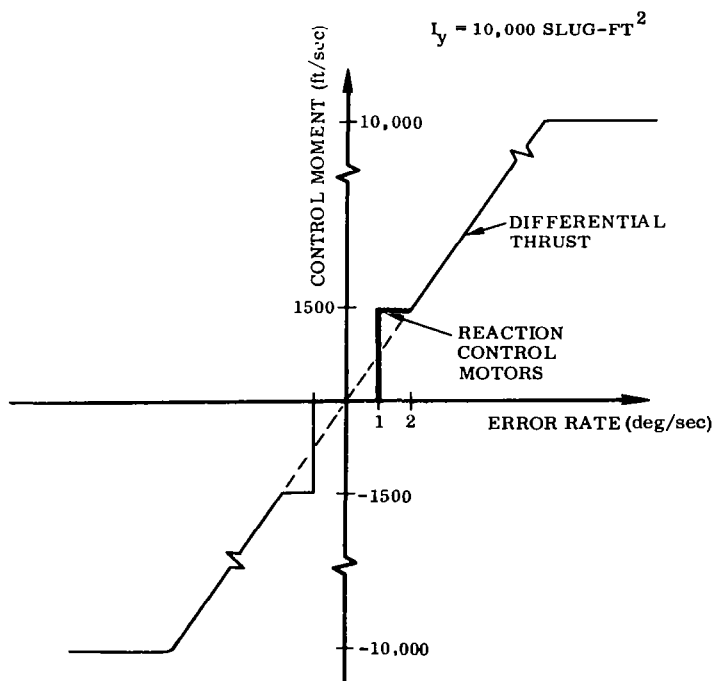


Figure 33. Total Control Moment as Function of Command

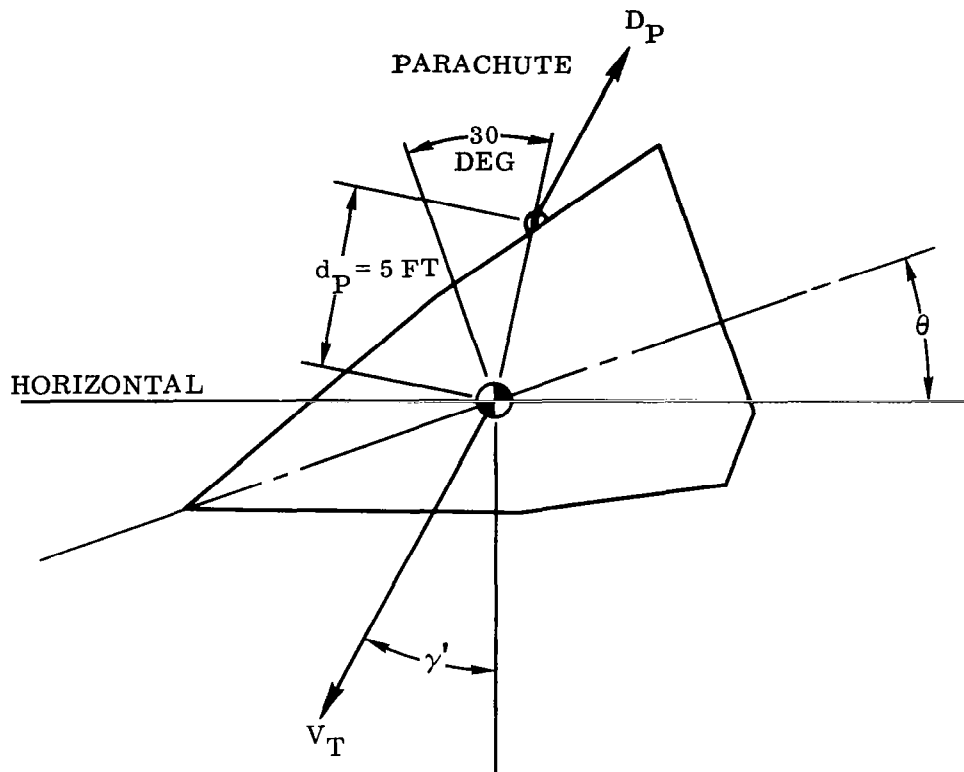


Figure 34. PLAME Parachute System

horizontal velocity. When the vehicle has attained a horizontal attitude and the sink rate is approximately 10 ft/sec, the parachute is jettisoned. Because of the horizontal velocity and the fact that a parachute tends to remain streamline, the jettisoned parachute is left clear of the vehicle. Another safety factor is that the unloaded parachute almost instantaneously reaches a steady-state sink rate of approximately 6 ft/sec. The parachute jettison is started at about 500 feet altitude and hover is attained at approximately 50 feet altitude.

**4.3.2 POWERED ROTORS.** The concept of using a folding rotor is a means of providing hard-ground landing capability for spacecraft and a means of assisting re-entry braking.

The use of a rotor for re-entry braking offers a number of potential advantages, among which are the possibility of tolerating steeper re-entry angles than could be tolerated by a fixed drag area body without excessive accelerations and the possibility of obtaining long supersonic glide ranges.

Figures 35 and 36 illustrate a possible rotor landing system installation for a typical ballistic spacecraft. The installation of the rotors does not involve any fundamental modifications to the spacecraft. The rotor installation is merely substituted for the parachute canister installation.

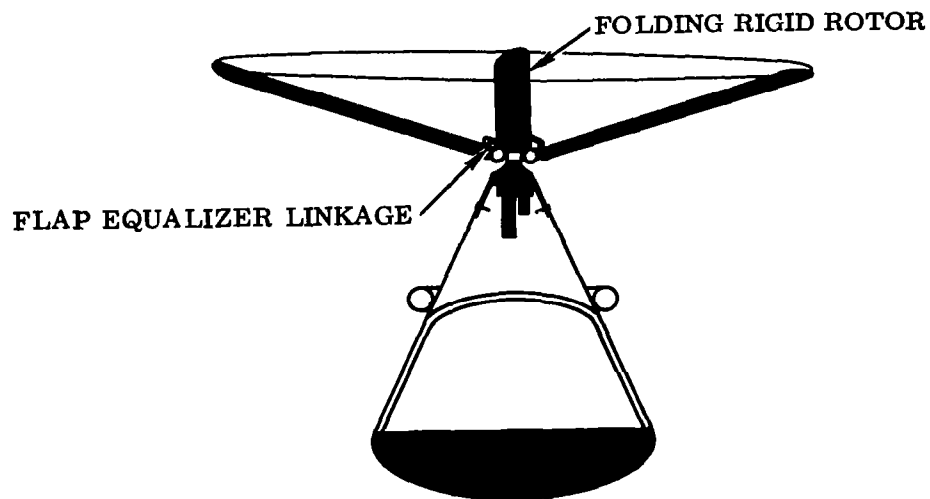


Figure 35. Rotor Landing System for One-Man Capsule, View 1

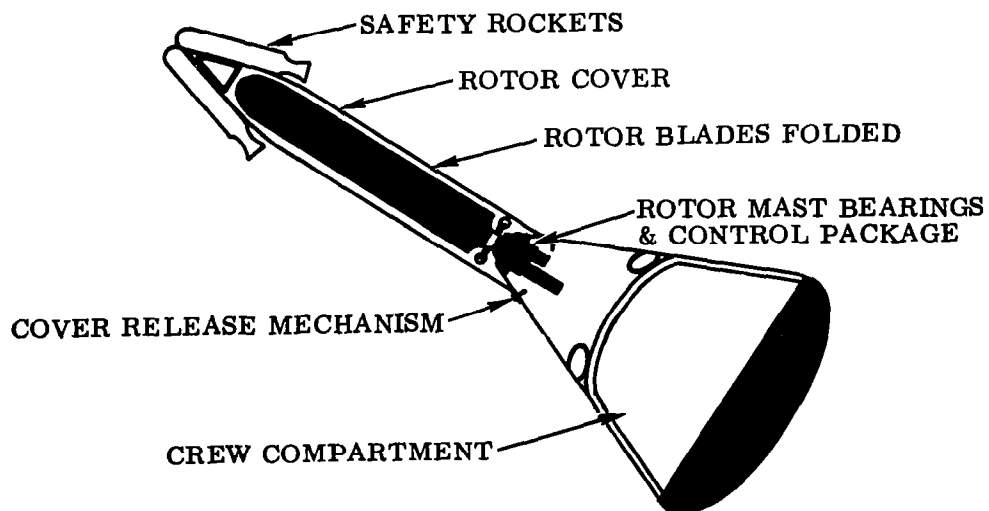


Figure 36. Rotor Landing System for One-Man Capsule, View 2

Figure 37 illustrates the sequence of operation of the rotor landing system during a re-entry maneuver. The rotor is deployed only after aerodynamic heating is no longer a major problem and, at first, would be used primarily as a drag-producing device in the trailing axial flow attitude.

After the rotor in the axial flow position has slowed the vehicle down to helicopter speeds, cyclic controls would be applied to the rotor and a helicopter type approach would be accomplished.

The final landing could be performed either with a conventional helicopter flared landing or with a vertical approach as illustrated in Figure 38. The helicopter-type flare landing would be preferred for a piloted vehicle since in this type of landing the pilot can keep the horizon in view while watching the landing spot, since pilot errors result primarily in horizontal residual velocity rather than vertical residual velocity.

Rotor opening in the axial attitude can be done entirely by aerodynamic forces, provided the rotor is pre-opened mechanically so that the blades project into the airstream and blade pitch is set to some angle other than flat pitch. Once there is a slight amount of rotation, centrifugal forces make the blade spread to a position giving larger forces. By means of collective pitch setting and selection of pre-opening angle, it is possible in the case of medium size rotors with normal blade weight (by helicopter standards) to adjust the opening rate anywhere from extremely fast to extremely slow.

Operation of a rotor in clean supersonic flight in the axial symmetric attitude does not appear to offer any fundamental theoretical difficulties. If any difficulties are encountered because of compressibility, it will probably be caused by the rotor operating in an irregular body wake at the transonic speeds at which the body is buffeting. This could be expected to lead to rotor vibrations as well as body vibrations.

Analysis of a rotor operating in the fully stalled propeller braking state indicates that a rotor in the trailing position will contribute to the directional stability of the vehicle, and maneuvering is accomplished by the usual helicopter cyclic pitch controls.

The problems of stability and control of a rotor system, powered or unpowered, are similar to those of conventional turbofan helicopters. These problems have been studied for considerable time.

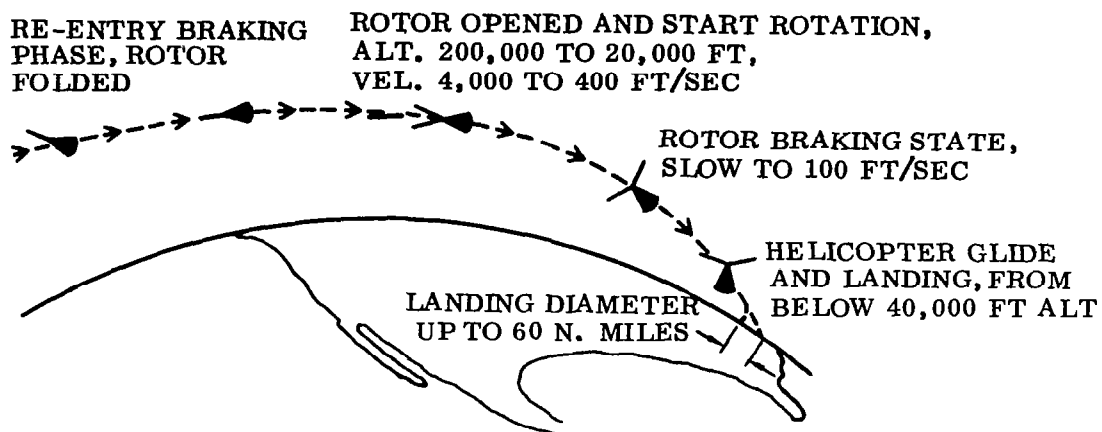


Figure 37. Rotor Landing System Operating Sequence

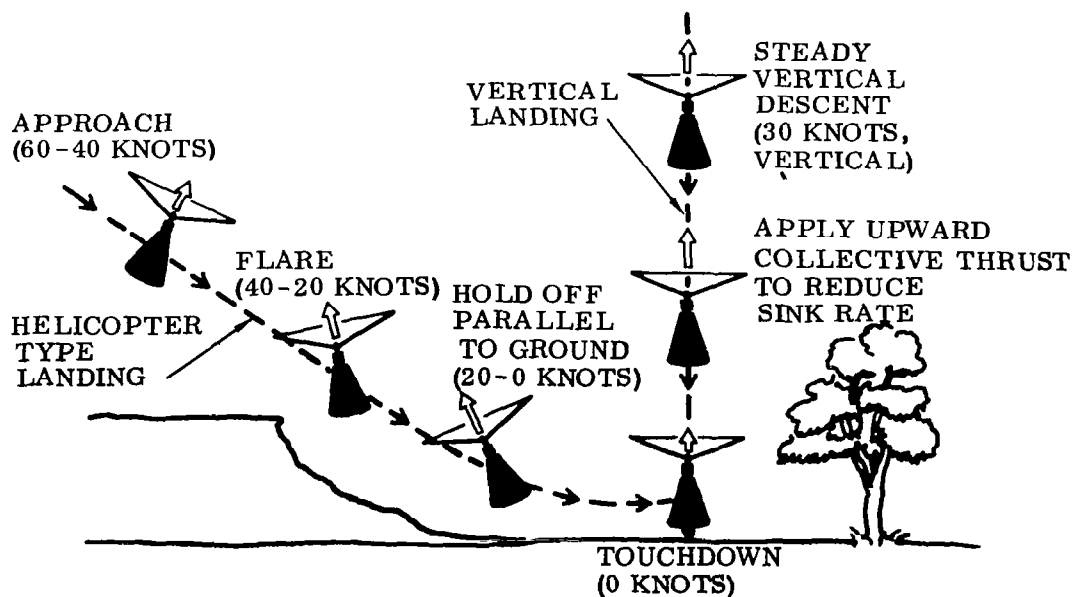


Figure 38. Landing Maneuvers with Rotor Landing System





## 5/REFERENCES

1. Steketee, F. D. , A Monograph on Entry Disturbance and Control,\* Convair division Report GDC-BTD67-023, 30 January 1967.
2. Bioastronautics Data Book, NASA SP-3006, Webb Associates, Yellow Springs, Ohio, 1964.
3. Knacke, T. N. , Development Status of the Steerable Cloverleaf Parachute, Northrop Ventura Report NVR-3830, April 1965.
4. Performance of and Design Criteria for Deployable Aerodynamic Decelerators, USAF-ASD-TR-61-579, December 1963.
5. Riley, V. F. , Final Report, Glidesail Development Program, Northrop Ventura Report PTM-524A, December 1962.
6. Symposium on Parachute Technology and Evaluation, USAF-FTC-TDR-64-12, September 1964.
7. Bray, R. S. , Drinkwater, F. J. , and White, M. D. , A Flight Study of a Power-Off Landing Technique Applicable to Re-Entry Vehicle, NASA TND-323, 1960.
8. Nelson, D. L. , Determination of Horizontal Landing Characteristics of Unpowered, Hypersonic Re-Entry Vehicle, Boeing Document D2-12746, November 1962.
9. Heinrich, H. G. , Drag and Stability of Parachutes, Aeronautical Engineering Review, June 1956, 73-81.
10. White, F. M. and Wolf, D. F. , A Theory of Three-Dimensional Parachute Dynamic Stability, AIAA Aerodynamic Deceleration System Conference, Houston, Texas, September 1966.
11. Lesko, J. S., Horizontal Landing of Piloted Lifting Re-Entry Vehicle, Boeing Company Report Aero-Space Division.
12. Mission Requirements of Lifting Systems - Engineering Aspects, McDonnell Report No. B831, August 1965.
13. Aviation Week and Space Technology, McGraw-Hill Publication, August 1967.
14. Myers, E. C. , Symposium on Parachute Technology and Evaluation, Proceedings Technical Documentary Report No. 64, September 1961.

---

\*A companion Design Criteria Monograph prepared for George C. Marshall Space Flight Center under Contract NAS8-11486.

15. Analytical Studies of the Use of the Propulsive-Lift Concept for the Descent and Landing of Manned Entry Vehicles, Convair division Report No. GDC-DCB67-015, May 1967.
16. Love, E. S. , "Manned Lifting Entry," Astronautics and Aeronautics, May 1966.

## APPENDIX

### A/PARACHUTE EQUATIONS OF MOTION AND STABILITY EQUATIONS

Appendix A presents the basic derivation of equations of motion along with simplified solutions to these equations for an earth landing spacecraft. This section presents first the assumptions used, next the basic equations, and finally solutions for both small disturbances and large disturbances.

#### A.1 ASSUMPTIONS

The following are the assumptions made for the equations and solutions to follow:

- a. The system consists of a symmetric parachute rigidly connected to a neutral payload.
- b. The aerodynamic forces and hydrodynamic inertia of the payload are negligible.
- c. There are five degrees of freedom, with the roll of the parachute about its axis of symmetry being ignored.
- d. The hydrodynamic mass and moment of inertia tensors of the canopy are approximated by single scalar values.
- e. The aerodynamic forces are assumed quasistatic based on the instantaneous angle of attack of the canopy.
- f. The canopy center of pressure is taken at the canopy centroid.
- g. A flat earth without wind is assumed.

These assumptions, while restrictive, still allow one to obtain considerable information about parachute stability.

#### A.2 EQUATIONS OF MOTION

A body axis system is used to compute linear velocities, angular velocities, aerodynamic forces and moments. An earth-fixed axis is used to compute the system trajectory. These two right-handed coordinate systems are illustrated in Figure A-1. The coordinate transformation is determined using the conventional Euler angle rotations.

##### A.2.1 BASIC DERIVATION.

$\psi$  = a rotation about Z

$\theta$  = a rotation about  $Y_2$  (position of  $Y_1$  after  $\psi$ )

$\phi$  = a rotation about  $X_3$  (position of  $X_1$  after  $\psi$  and  $\theta$ )

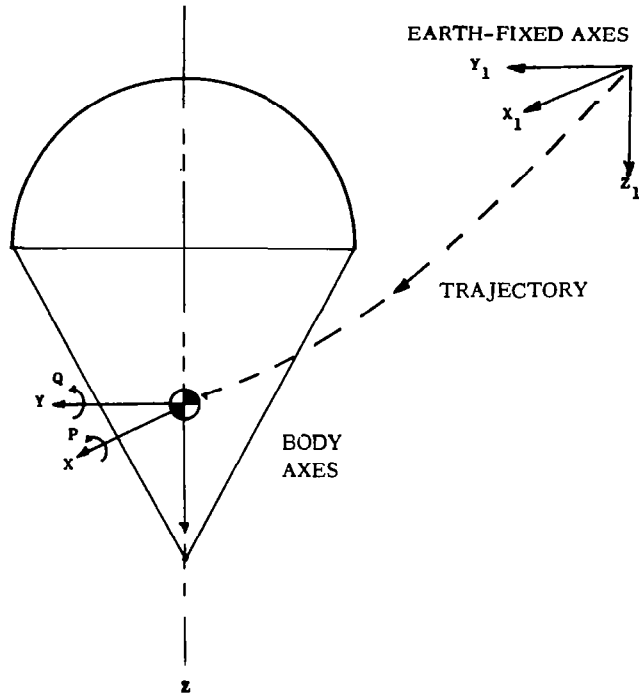


Figure A-1. Coordinate Systems

The five force and moment equations in the body axis system then become:\*

$$\begin{aligned}
 m(\dot{U} + QW) &= X - (m_p + m_c)gs\theta \\
 m(\dot{V} - PW) &= Y + (m_p + m_c)gc\theta s\phi \\
 m(\dot{W} - QU) &= Z + (m_p + m_c)gc\theta c\phi \\
 I(\dot{P}) &= M - m_p gL_p c\theta s\phi + m_c gL_c c\theta s\phi \\
 I(\dot{Q}) &= N + s\theta (m_c gL_c - m_p gL_p)
 \end{aligned} \tag{A-1}$$

where  $m = (m_p + m_c + m_{cn})$  and  $I = (I_p + I_c + I_{cn})$  include the hydrodynamic or apparent inertia of the canopy. The body angular velocities are related to the Euler angle by the expressions

$$\begin{aligned}
 \dot{\theta} &= Qc\phi \\
 \dot{\phi} &= P + Qs\phi T\theta \\
 \dot{\psi} &= Qs\phi/c\theta
 \end{aligned} \tag{A-2}$$

\*The terms (s and c) are used for abbreviations of sine and cosine for brevity in equations A-1 through A-5.

The lengths  $L_c$  and  $L_p$  relate the centroid of the canopy and payload to the system centroid as shown in Figure A-2. Since the canopy is assumed to provide all of the aerodynamic forces and moments, the angle of attack is taken to be the instantaneous angle  $\alpha$  between the velocity  $V_c$  of the canopy centroid and the axis of symmetry  $Z$  as shown in Figure A-2.

For the trajectory of the system centroid in earth-fixed coordinates

$$\begin{aligned}\dot{X}_1 &= U c \theta c \psi + V (s \phi s \theta c \psi - c \phi c \psi) + W (c \phi s \theta c \psi + s \phi s \psi) \\ \dot{Y}_1 &= U c \theta s \psi + V (s \phi s \theta s \psi + c \phi c \psi) + W (c \phi s \theta s \psi - s \phi c \psi) \\ \dot{Z}_1 &= U s \theta + V s \phi c \theta + W c \phi c \theta\end{aligned}\tag{A-3}$$

Only Equations (A-1) and A-2) are needed for a stability study.

A.2.2 NONDIMENSIONAL EQUATION. To make Equation (A-1) nondimensional in system length and steady-state glide speed (see Figure A-3),  $L$  and  $V_o$  are used:

$$\begin{aligned}u &= \frac{U}{V_o}; v = \frac{V}{V_o}; w = \frac{W}{V_o} \\ p &= \frac{L P}{V_o}; q = \frac{L Q}{V_o}; t^* = \frac{V_o t}{L}\end{aligned}\tag{A-4}$$

Substitution into Equations (A-1) give the following dimensionless equations of motion:

$$\begin{aligned}Du &= \frac{-C_n V_c^{*2} \left(u - \frac{g}{1+r_c}\right)}{2k \sqrt{V_c^{*2} - w^2}} - \frac{C_{T_o}}{2k} s \theta - g w \\ Dv &= \frac{-C_n V_c^{*2} \left(v + \frac{p}{1+r_c}\right)}{2k \sqrt{V_c^{*2} - w^2}} + \frac{C_{T_o}}{2k} c \theta s \phi + p w \\ Dw &= \frac{-C_T V_c^{*2}}{2k} + \frac{C_{T_o}}{2k} c \theta c \phi - P v + g u\end{aligned}\tag{A-5}$$

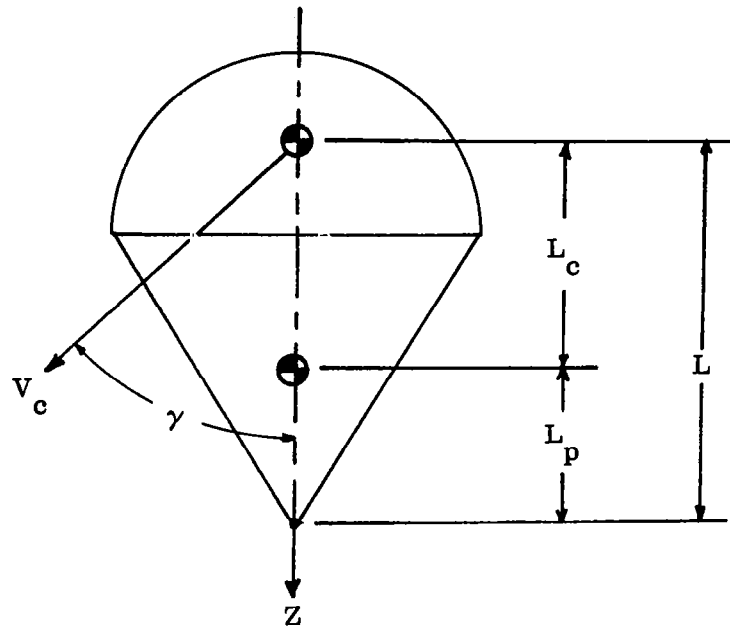


Figure A-2. Angle of Attack and Centroidal Lengths

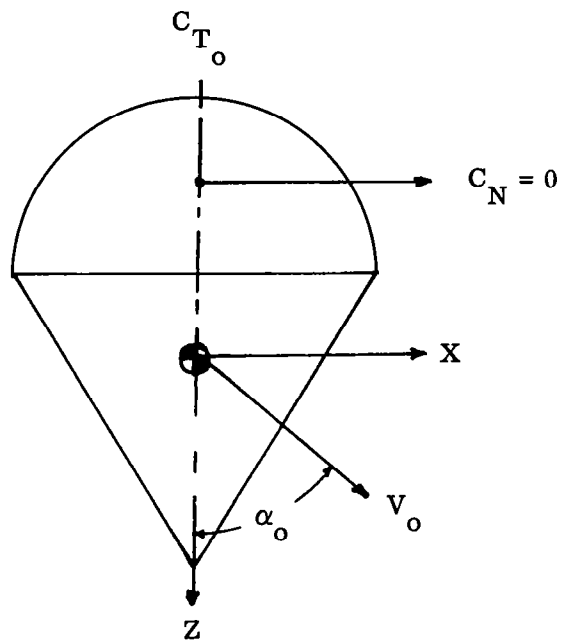


Figure A-3. Statically Stable Glide

$$Dp = \frac{-C_n V_c^{*2} \left( v = \frac{p}{1+r_c} \right)}{2i(1+r_c) \sqrt{V_c^{*2} + w^2}} - \frac{C_{T_o} r_{c_h}}{2i(1+r_c)}$$

$$Dq = \frac{C_n V_c^{*2} \left( u = \frac{q}{1+r_c} \right)}{2i(1+r_c) \sqrt{V_c^{*2} - w^2}} - \frac{C_{T_o} V_{c_h}}{2i(1+r_c)} \sin \theta$$

$$V_c^{*2} = w^2 + \left( u - \frac{q}{1+r_c} \right)^2 + \left( v + \frac{p}{1+r_c} \right)^2$$

The dimensionless parameters in Equations (A-5) are the following:

$$r_c = \frac{m_c + m_{c_h}}{m_p} \quad ; \quad r_{c_h} = \frac{m_{c_h}}{m_c + m_p}$$

$$K = \frac{m}{\rho A L} \quad ; \quad i = \frac{I}{\rho A L^3} j \quad (A-6)$$

$$C_{T_o} = \frac{(m_c + m_p)g}{1/2 \rho V_o^3 A} \quad ; \quad C_N = \frac{X^2 + Y^2}{1/2 \rho V_o^2 A} \quad ;$$

$$C_T = \frac{-Z}{1/2 \rho V_o^2 A}$$

The quantities  $C_N$  and  $C_T$  are the normal and tangential aerodynamic force coefficients of the chute and depend upon the instantaneous angle of attack  $\alpha$  of the canopy:

$$\alpha = \tan^{-1} \left\{ \frac{1}{w} \sqrt{\left( \mu - \frac{q}{1+r_c} \right)^2 + \left( v + \frac{p}{1+r_c} \right)^2} \right\} \quad (A-7)$$

The quantity  $V_c^*$  is the dimensionless velocity of the canopy. Equations (A-2), (A-3), and (A-5) constitute the complete set of dimensionless equations of motion.

### A.3 SOLUTIONS OF EQUATIONS OF MOTION

For purposes of presenting and discussing solutions, the equations of motion have been broken into two general categories: solutions for small disturbances and solutions in the presence of large disturbances.

**A.3.1 SMALL DISTURBANCE ANALYSIS.** Because of the unusual shape of the force coefficient curves, most parachutes do not fall vertically, even if they are very stable. Figure A-4 is a sketch of typical parachute aerodynamic coefficients as a function of angle of attack. Note that the  $C_N$  curve is antisymmetric to account for the change in direction of the normal force, which is acting away from the centerline if  $\alpha$  is between  $-\alpha_0$  and  $+\alpha_0$ . A parachute cannot remain at the point ( $\alpha = 0$ ), even though the normal force is zero there, because any shift disturbance will drive the chute away from the origin due to the outward acting normal force at slight angle of attack. This condition is termed "static instability" and will be derived vigorously here. However, as discussed by Heinrich (Reference 9) the point ( $\alpha = \alpha_0$ ) is statically stable since a slight disturbance causes a normal force which returns the chute back toward  $\alpha_0$ . Heinrich calls  $\alpha_0$  the "stable glide point", because the chute will glide with its tangent force exactly balancing the system weight, as shown in Figure A-3. Unfortunately, as we shall see, the glide point, while statically stable, may be dynamically unstable, so that a given parachute may be unable to continue gliding and instead may oscillate or perform a coning motion.

To investigate linearized stability of the glide point we assume small disturbances from a steady glide in the X-Z plane. Then the reference state is:

$$\begin{aligned} \alpha &= \alpha_0 ; C_T = C_{T_0} ; C_N = 0 ; n_0 = \sin \alpha ; v = 0 ; \\ w_0 &= \cos \alpha_0 ; p = g = \theta = \phi = 0 \end{aligned} \quad (A-8)$$

Then defining the disturbance variables by primes:

$$\begin{aligned} u' &= u - u_0 ; v' = v ; w' = w - w_0 ; p' = p ; g' = g \\ \theta' &= \theta ; \phi' = \phi \end{aligned} \quad (A-9)$$

Assume that the force coefficients are approximated by straight lines in the neighborhood of the glide point, as shown by the dotted lines in Figure A-4

$$\alpha' = \alpha - \alpha_0 \quad (A-10)$$



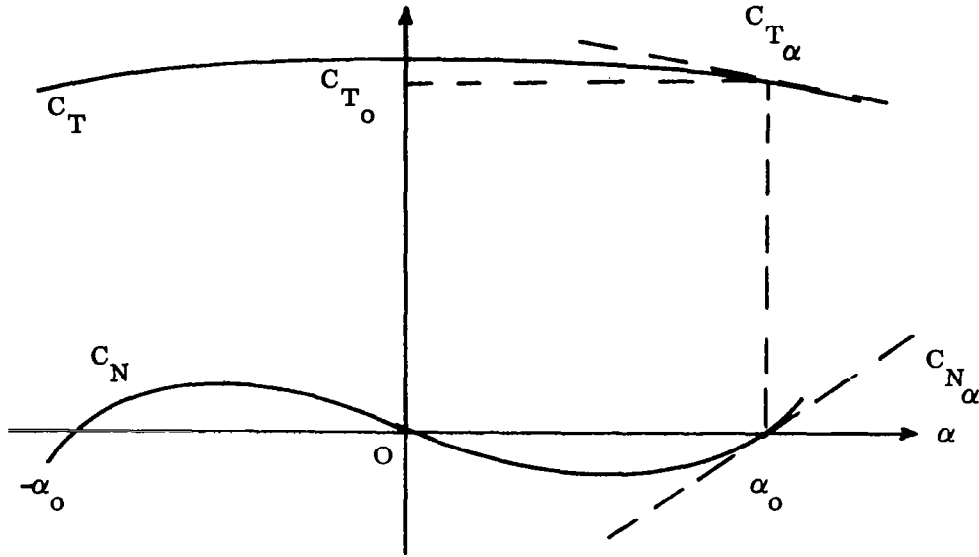


Figure A-4. Typical Force Coefficient Curves for a Parachute

$$C_N = C_{N_\alpha} \alpha' \quad (A-10)$$

$$C_T = C_{T_0} + C_{T_\alpha} \alpha'$$

Substitute Equations (A-9) and (A-10) into Equation (A-5) and neglect squares and higher powers of disturbance variables. The following linearized equations of motion can be written about the glide point:

$$\left( D + \frac{C_{N_\alpha} c \alpha_0}{2k} \right) \mu' - \frac{C_{N_\alpha} s \alpha_0}{2k} w' + \left( \left( C_{\alpha_0} - \frac{C_{N_\alpha} c \alpha_0}{2k(1+r_c)} \right) D + \frac{C_{T_0}}{2k} \right) \theta = 0 \quad (A-11)$$

$$\left( \frac{C_{T_\alpha} c \alpha_0 + 2C_{T_0} s \alpha_0}{2k} \right) \mu' + \left( D + \frac{2C_{T_0} c \alpha_0 - C_{T_\alpha} s \alpha_0}{2k} \right) w' + \left( s \alpha_0 - \frac{C_{T_\alpha} c \alpha_0 + 2C_{T_0} s \alpha_0}{2k(1+r_c)} \right) D \theta' = 0 \quad (A-12)$$

$$\begin{aligned}
& -\frac{C_{N\alpha} c \alpha_o}{2i(1+r_c)} u' + \frac{C_{N\alpha} s \alpha_o}{2i(1+r_c)} w' + \left( D^2 + \frac{C_{N\alpha} c \alpha_o}{2i(1+r_c)^3} D \right. \\
& \left. + \frac{C_{T_o} r_{ch}}{2i(1+r_c)} \right) \theta' = 0
\end{aligned} \tag{A-13}$$

$$D v' - \left( c \alpha_o D + \frac{C_{T_o}}{2k} \right) \phi' = 0 \tag{A-14}$$

$$\left( D^2 + \frac{C_{T_o} r_{ch}}{2i(1+r_c)} \right) \phi' = 0 \tag{A-15}$$

where

$$D \text{ is } \frac{d}{dt^*}$$

These linearized equations have the valuable property that the longitudinal and lateral motions are uncoupled. This uncoupling is similar to that found in the study of aircraft linearized stability.

**A.3.1.1 Longitudinal Stability.** Since Equation (A-11), (A-12), and (A-13) are linear with constant coefficients, the solution must be the exponential form  $e^{\lambda t^*}$  where  $\lambda$  is a constant. The determinant of the coefficient leads to the fourth order algebraic equation for the constant  $\lambda$ :

$$\lambda^4 + C_1 \lambda^3 + C_2 \lambda^2 + C_3 \lambda + C_4 = 0 \tag{A-16}$$

$$C_1 = E_1 C_{N\alpha} + E_2$$

$$C_2 = E_3 C_{N\alpha} + E_4$$

$$C_3 = E_5 C_{N\alpha} + E_6$$

$$C_4 = E_7 C_{N\alpha} \tag{A-17}$$

and the constants  $E_i$  are:

$$\begin{aligned}
 E_1 &= \frac{c\alpha_o \left( k+i (1+r_c)^2 \right)}{2ki (1+r_c)^2} \\
 E_2 &= \frac{2C_{T_o} c\alpha_o - C_{T_\alpha} s\alpha_o}{2k} \\
 E_3 &= \frac{C_{T_o} \left( k+i (1+r_c)^2 + k^2 (1+r_c) \right)}{2k^2 i (1+r_c)^2} \\
 E_4 &= \frac{C_{T_o} r_{ch}}{2i(1+r_c)} \\
 E_5 &= \frac{C_{T_o} c\alpha_o (3+r_{ch})}{4ki (1+r_c)} \\
 E_6 &= \frac{C_{T_o} r_{ch} \left( 2C_{T_o} c\alpha_o - C_{T_\alpha} s\alpha_o \right)}{4ki (1+r_c)} \\
 E_7 &= \frac{C_{T_o}^2 (1+r_{ch})}{4k^2 i (1+r_c)} \tag{A-18}
 \end{aligned}$$

For stability, it is necessary that  $C_4$  be positive, which is true if  $C_{N\alpha}$  is positive, since  $E_7$  is always positive.

For dynamic stability the real parts of the four roots must all be negative or

$$C_1, C_2, C_3 \text{ and } C_4 > 0 \tag{A-19}$$

and

$$C_3(C_1 C_2 - C_3) - C_1^2 C_4 > 0$$

$$C_3 - C_1 C_2 > 0 \quad (A-20)$$

Equations (A-19) and (A-20) are obtained using the Ronthe-Howitz stability criterion. Equation (A-19) is also satisfied if  $C_{N\alpha}$  is positive, a condition already required.

Equation (A-20) leads to a quadratic equation in  $C_{N\alpha}$ :

$$K_1 C_{N\alpha}^2 + K_2 C_{N\alpha} + K_3 \geq 0 \quad (A-21)$$

$$K_1 = E_1 (E_3 E_5 - E_1 E_7)$$

$$K_2 = E_5 (E_2 E_3 - E_1 E_4 - E_5) + E_1 (E_3 E_6 - 2E_2 E_7)$$

$$K_3 = E_2 (E_4 E_5 - E_3 E_6 - E_2 E_7) + E_6 (E_1 E_4 - 2E_5) \quad (A-22)$$

Equation (A-21) yields the minimum value  $C_{N\alpha}(\min)$  required for dynamic stability:

$$C_{N\alpha}(\min) = -\frac{K_2}{2K_1} + \sqrt{\frac{K_2^2}{4K_1^2} - \frac{K_3}{K_1}} \quad (A-23)$$

**A.3.1.2 Numerical Stability Results.** The parameters  $k$ ,  $i$ ,  $r_c$  and  $r_{ch}$  are not very significant physically, because the hydrodynamic inertia is mixed into all of them. Consider the following:

$V_o^2/gL$  = descent Froude number

$D_o/L$  = the chute slenderness ratio

$m_c/m_p$  = the canopy-to-load mass ratio

$C_{T_o}$  = the gliding force coefficient

$D_o$  = the nominal diameter of the canopy

The dimensionless hydrodynamic inertias  $B_m$  and  $B_i$  are defined as:

$$B_m = \frac{6m_{ch}}{\pi \rho D_o^3}$$

$$B_i = \frac{60 I_{ch}}{\pi \rho D_o^5} \quad (A-24)$$

The hydrodynamic inertia factors have been measured experimentally and are shown in Figure A-5 as a function of geometric porosity.

The effect of  $C_T$  on stability is small except at large  $\alpha_o$ . Many parachutes, particularly glide-surface types, have zero  $C_{T\alpha}$ . If the assumption that  $C_{T\alpha} = 0$  is made then Equations (A-13), (A-14), (A-15) greatly simplify. The determinant of coefficients reduces to a cubic:

$$\lambda^3 + C_1 \lambda^2 + C_2 \lambda + C_3 = 0$$

$$C_1 = 1/2 C_{N\alpha} \left( \frac{1}{k} + \frac{1}{i(r+r_c)^2} \right) \quad (A-25)$$

$$C_2 = \frac{C_{N\alpha} + C_{T_o} r_{ch}}{2i(1+r_c)}$$

$$C_3 = \frac{C_{N\alpha} C_{T_o} (1+r_{ch})}{4ki(1+r_c)} \quad (A-26)$$

which is independent of the angle  $\alpha_o$ . The stability criterion is that  $C_1 C_2 = C_3$ , which results in a very simple expression for  $C_{N\alpha}(\min)$ :

$$C_{N\alpha}(\min) = \frac{C_{T_o} \left( i(1+r_c)^2 - kr_{cn} \right)}{i(1+r_c)^2 + k} \quad (A-27)$$

Figure A-6 shows wind tunnel measurements of  $C_{N\alpha}$  and  $C_{T\alpha}$  for three different parachute shapes.

Figure A-7 illustrates the general result that a heavily loaded chute is more stable than the lightly loaded system. It also shows the effect of  $\alpha_o$  and  $C_{T\alpha}$  on stability. Setting  $C_{T\alpha} = 0$  is conservative, or, in a sense, negative  $C_{T\alpha}$  has a stabilizing effect at final glide angles.

Figure A-8 indicates that a slowly descending parachute is less stable than a more rapidly descending parachute.

Figure A-9 shows the general effect of slenderness ratio. As might be expected, a parachute with long line (small  $D_o/L$ ) is more stable.

**A.3.1.3 Lateral Dynamic Stability.** The lateral motion, Equations (A-16) and (A-17), is much simpler and yields the following stability polynomial:

$$\frac{\lambda \left( \lambda^2 + C_{T_o} r_{ch} \right)}{2i(1+r_c)} = 0 \quad (A-28)$$

The real part of all three roots is obviously zero. Hence lateral small disturbances will lead to neutrally stable oscillations. The linear analysis predict no coning.

**A.3.2 LARGE DISTURBANCE.** To indicate the limitations of the preceding linearized analysis, some exact computer solutions of Equation (A-5) will be shown.

**A.3.2.1 Longitudinal Disturbances.** Figure A-10 shows the response  $\theta'(t^*)$  from the computer solution for each of three disturbances:  $1^\circ$ ,  $10^\circ$  and  $20^\circ$ . The  $1^\circ$  disturbance is in nearly perfect agreement with the linear theory. The  $10^\circ$  disturbance still damps out but at a lesser rate. In contrast the  $20^\circ$  disturbances case does not damp out but instead jumps to a large angle ( $\pm 32^\circ$ ) oscillation which persists.

**A.3.2.2 Lateral Disturbances.** The lateral behavior of the system can be observed by comparing two disturbances,  $\phi' = 1^\circ$  and  $40^\circ$ . The resulting responses are shown in Figure A-11. For the  $1^\circ$  disturbance the response is in good agreement with linear theory and the induced longitudinal motion  $\theta$  is negligible.

In contrast, the large disturbance of  $40^\circ$  immediately induces a longitudinal motion  $\theta$  of comparable magnitude. The canopy is falling directly downward, while the load is moving downward along a helical path of constant radius. In short the  $40^\circ$  lateral disturbance has thrown the parachute into a uniform vertical coning motion.

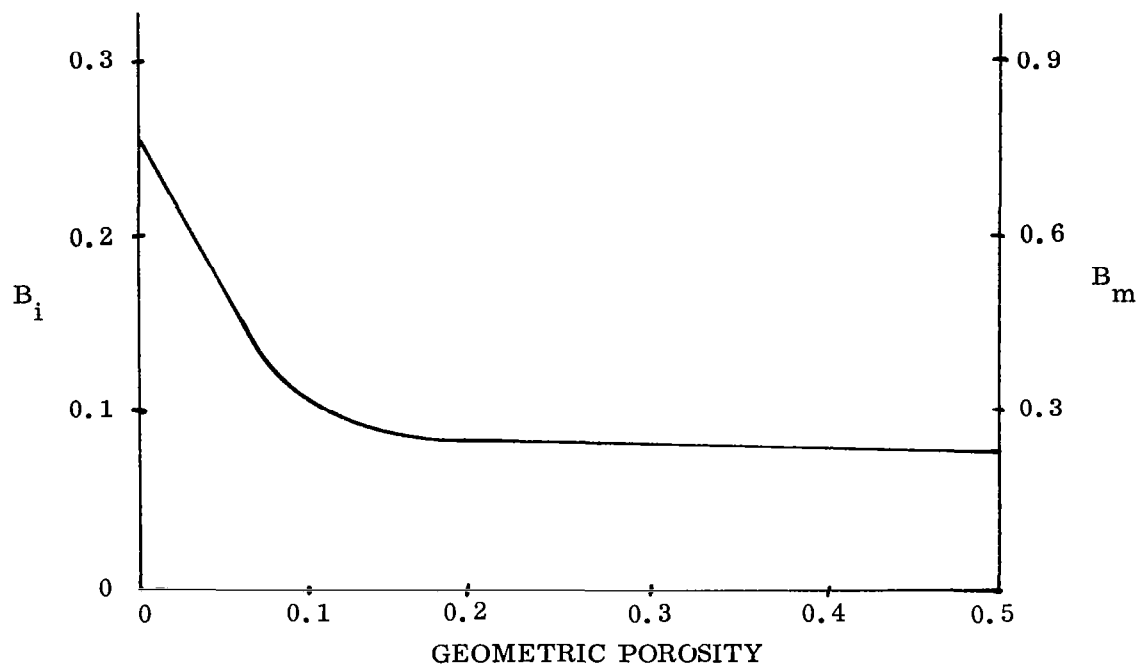


Figure A-5. Nondimensional Apparent Inertia

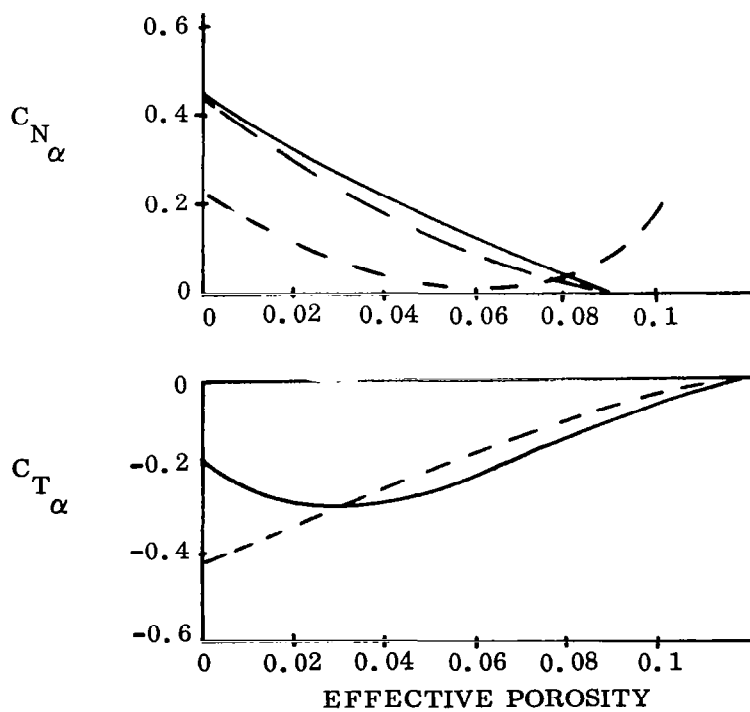


Figure A-6. Experimental Curves for  $C_{N\alpha}$  and  $C_{T\alpha}$  per Radian

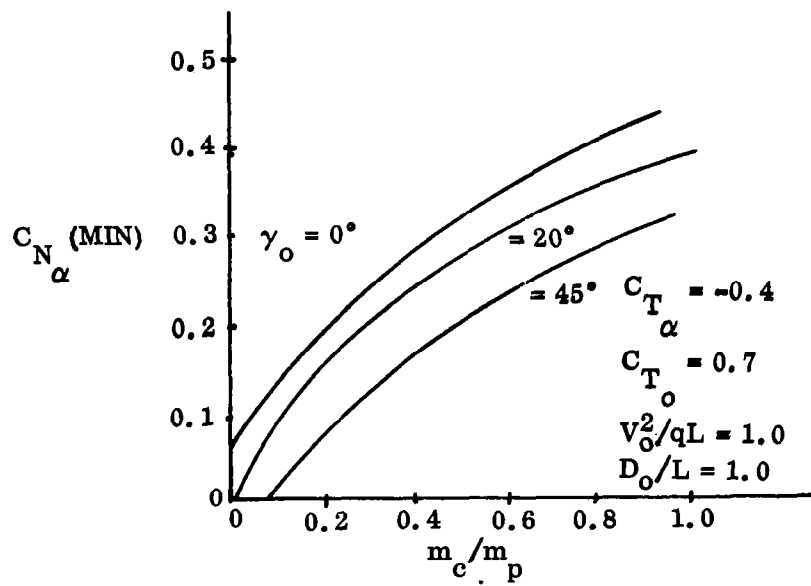


Figure A-7. Effects of Glide Angle on Stability

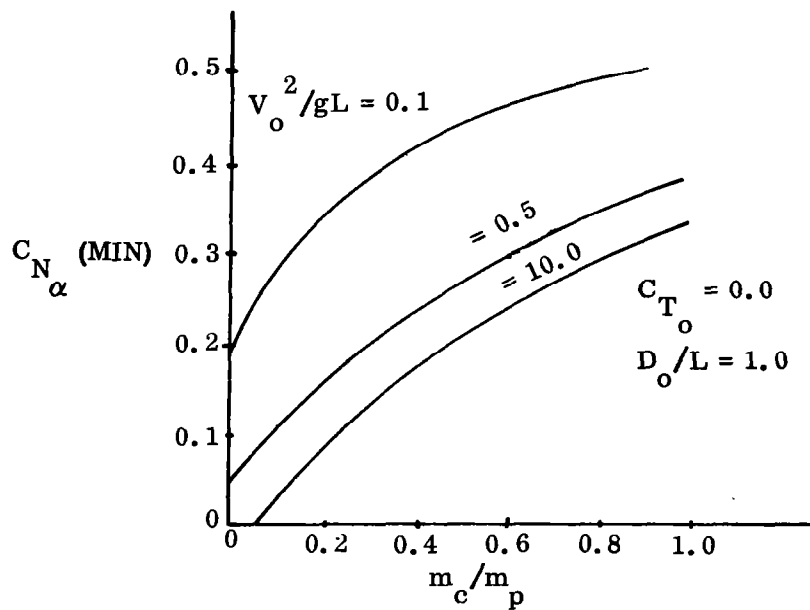


Figure A-8. Effects of Froude Number on Stability



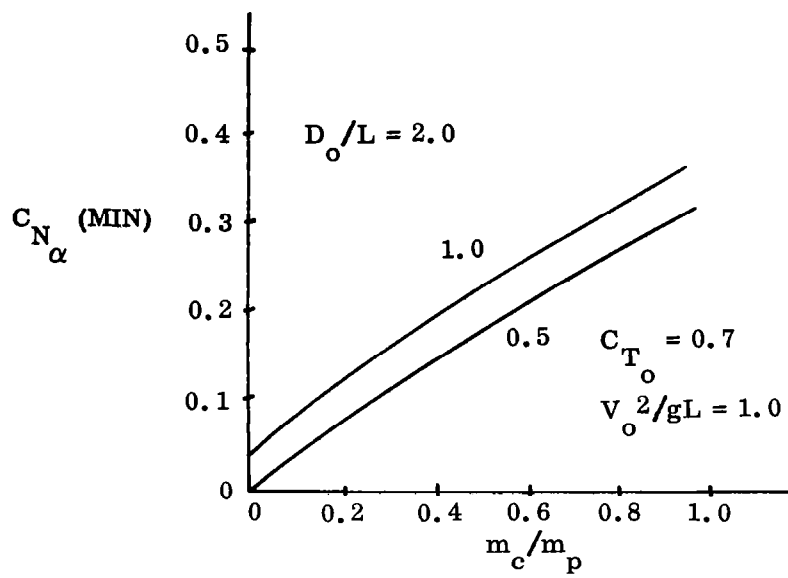


Figure A-9. Effects of Slenderness Ratio on Stability

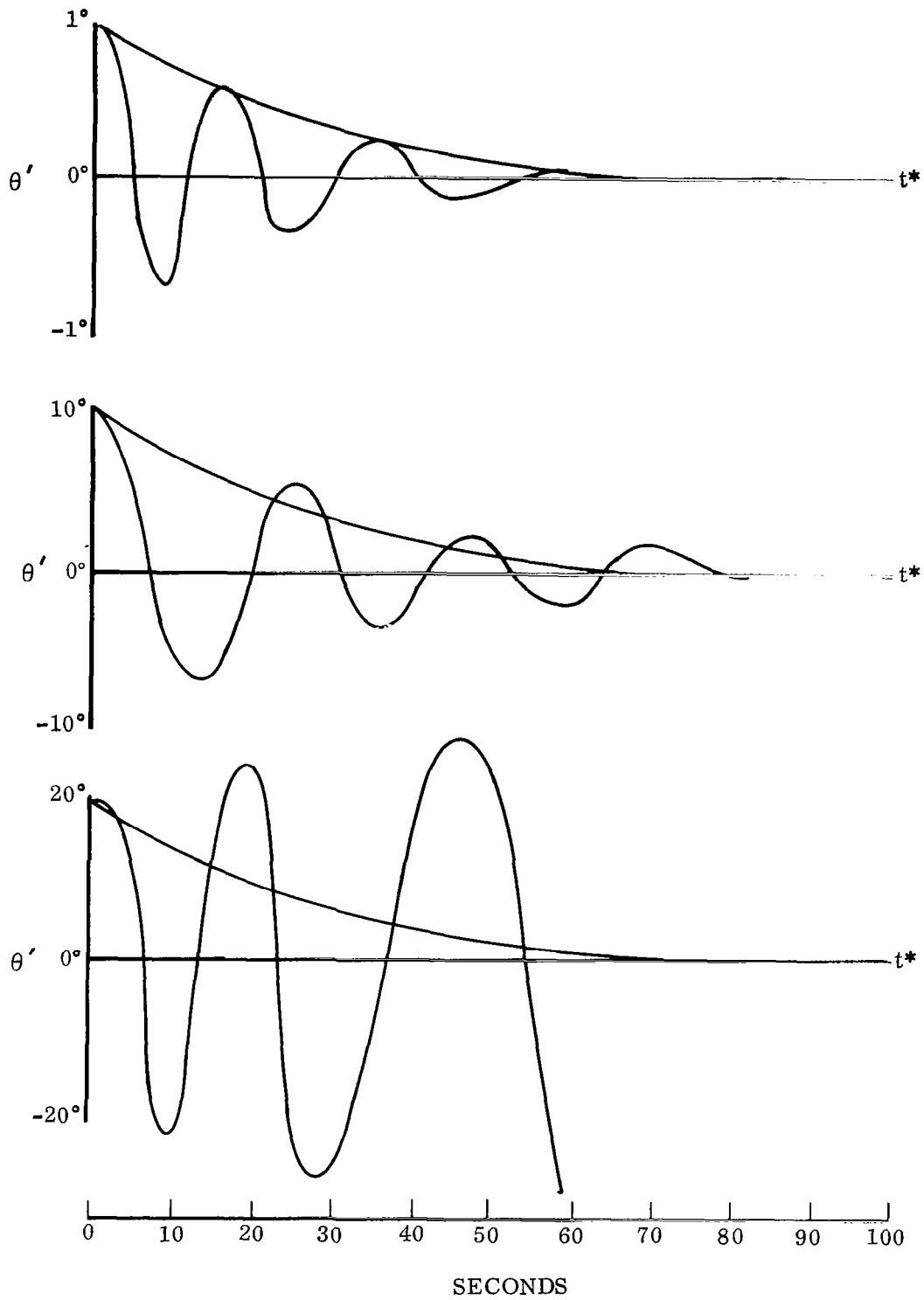


Figure A-10. Computer Simulation for  $1^\circ$ ,  $10^\circ$  and  $20^\circ$  Disturbances

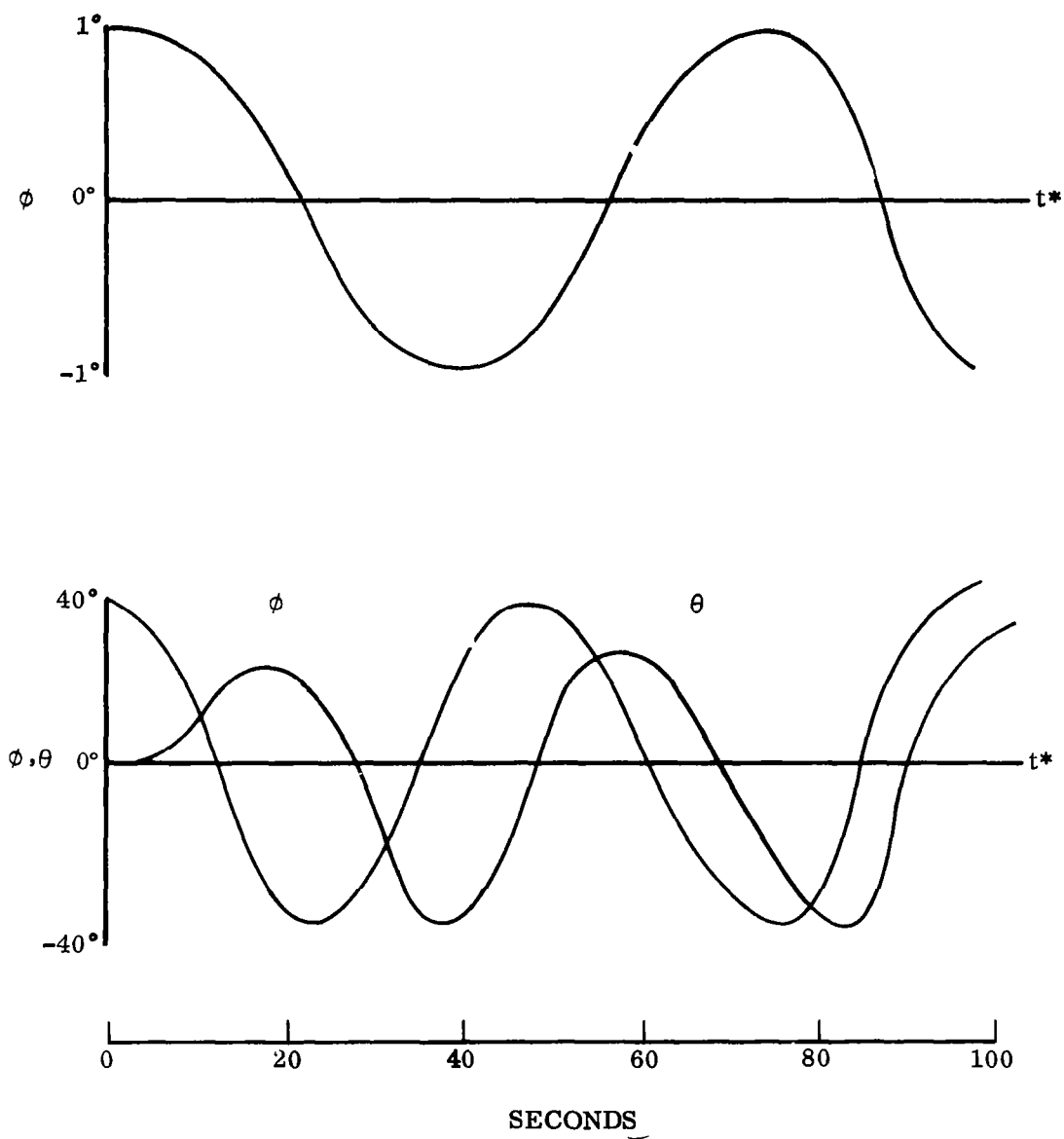


Figure A-11. Response to  $1^\circ$  and  $40^\circ$  Lateral Disturbance

05U 001 57 51 3DS 68120 00903  
AIR FORCE WEAPONS LABORATORY/AFWL/  
KIRTLAND AIR FORCE BASE, NEW MEXICO 87117

ATT MISS MADELINE F. CANOVA, CHIEF TECHNICAL  
LIBRARY /WLIL/

POSTMASTER: If Undeliverable (Section 158  
Postal Manual) Do Not Return

*"The aeronautical and space activities of the United States shall be conducted so as to contribute . . . to the expansion of human knowledge of phenomena in the atmosphere and space. The Administration shall provide for the widest practicable and appropriate dissemination of information concerning its activities and the results thereof."*

— NATIONAL AERONAUTICS AND SPACE ACT OF 1958

## NASA SCIENTIFIC AND TECHNICAL PUBLICATIONS

**TECHNICAL REPORTS:** Scientific and technical information considered important, complete, and a lasting contribution to existing knowledge.

**TECHNICAL NOTES:** Information less broad in scope but nevertheless of importance as a contribution to existing knowledge.

**TECHNICAL MEMORANDUMS:** Information receiving limited distribution because of preliminary data, security classification, or other reasons.

**CONTRACTOR REPORTS:** Scientific and technical information generated under a NASA contract or grant and considered an important contribution to existing knowledge.

**TECHNICAL TRANSLATIONS:** Information published in a foreign language considered to merit NASA distribution in English.

**SPECIAL PUBLICATIONS:** Information derived from or of value to NASA activities. Publications include conference proceedings, monographs, data compilations, handbooks, sourcebooks, and special bibliographies.

**TECHNOLOGY UTILIZATION PUBLICATIONS:** Information on technology used by NASA that may be of particular interest in commercial and other non-aerospace applications. Publications include Tech Briefs, Technology Utilization Reports and Notes, and Technology Surveys.

*Details on the availability of these publications may be obtained from:*

SCIENTIFIC AND TECHNICAL INFORMATION DIVISION  
NATIONAL AERONAUTICS AND SPACE ADMINISTRATION  
Washington, D.C. 20546